2022

Microglia Distribution in the Lateral Ventricles Following Treatment of Lysolecithin Model of Multiple Sclerosis

Spencer James Wilson
Wright State University

MICROGLIA DISTRIBUTION IN THE LATERAL VENTRICLES FOLLOWING TREATMENT OF LYSOLECITHIN MODEL OF MULTIPLE SCLEROSIS

A thesis submitted in partial fulfillment of the
requirements for the degree of
Master of Science

by

SPENCER JAMES WILSON

B.S., Wright State University, 2021

2022

Wright State University

WRIGHT STATE UNIVERSITY

GRADUATE SCHOOL

July 29, 2022

I HEREBY RECOMMEND THAT THE THESIS PREPARED UNDER MY SUPERVISION BY Spencer James Wilson ENTITLED Microglia distribution in the lateral ventricles following treatment of lysolecithin model of Multiple Sclerosis BE ACCEPTED IN PARTIAL FULFILLMENT OF THE REQUIREMENTS FOR THE DEGREE OF Master of Science.

_____

Adrian Corbett, Ph.D.
Thesis Director

_____

Eric Bennet, Ph.D.
Chair, Department of Neuroscience,
Cell Biology, and Physiology

Committee on Final Examination:

_____

Adrian Corbett, Ph.D.

_____

Christopher Wyatt, Ph.D.

_____

Keiichiro Susuki, M.D., Ph.D.

_____

Barry Milligan, Ph.D.
Dean of the Graduate School

ABSTRACT

Wilson, Spencer James. M.S., Department of Neuroscience, Cell Biology, and Physiology, Wright State University, 2022. "Microglia distribution in the lateral ventricles following treatment of lysolecithin model of Multiple Sclerosis"

Multiple sclerosis (MS) affects an estimated one million people in the US alone (Wallin et al., 2019). We modeled MS in rats using lysolecithin injection into the corpus callosum to diminish motor function unilaterally through demyelination, meanwhile treating the injury with Fluoxetine, Ibuprofen, and ascorbic acid (FIAA) to increase neurogenesis and oligodendrogenesis. Motor function was assessed using the Montoya Staircase test pre- and post-surgery. Motor capabilities recovered in the contralateral limb, but not in the ipsilateral, and recovery was not significantly affected by treatment. We identified microglia by CX3CR1 and examined its distribution in the adult neurogenic niche, the SVZ of the lateral ventricles. Microglia displayed significant regional differences with posterior ventricle slices containing more microglial area than those of the anterior, and the treatment had no significant effect on this distribution. We found CX3CR1 area to be more negatively correlated with functional recovery in treated animals compared to controls, indicating that the treatment may favor recovery in animals with a greater proportion of activated microglia.

TABLE OF CONTENTS

LIST OF FIGURES

Page

LIST OF TABLES

Page

I. INTRODUCTION

Multiple Sclerosis

Multiple sclerosis (MS) is a demyelinating disease of the central nervous system characterized by autoimmune attack on myelin. The disease affects an estimated one million people in the US alone. Large-scale studies have shown a strong sex bias in MS that skews disease prevalence toward females approximately 3:1 (Wallin et al., 2019), indicating a possible estrogen-dependent mechanism. Additionally, the age group with the highest MS prevalence, 55-64, is concomitant with the progression of menopause (Wallin et al., 2019). Therefore, it is apparent that examining the effects of enhancing estrogen-dependent pathways that might be involved in MS pathology could yield therapeutic benefits.

Diagnosing MS can be a rigorous undertaking. Usually diagnosed in young adults, the disease often presents with both demyelinated inflammation and neurodegeneration with gliosis, commonly in white matter tracts such as the corpus callosum. Patients can experience chronic pain, fatigue, ambulatory problems, and severe dysfunction in fine motor skills (Squillace & Linden, 2022; Gustavsen et al., 2021). Patients may have severe episodes of symptoms that take six months to diagnose. Part of this delay is the requirement for a “dissemination in time and space” of disease

hallmarks. Two demyelinating lesions found by magnetic resonance imaging (MRI) must be identified at least one month apart and distinct from one another (Hauser and Cree, 2020). At each time point, patients must have symptoms lasting 24 hours or longer. If one lesion is identified with acute and anatomically focused symptoms, the patient may be diagnosed with clinically isolated syndrome (CIS), a recent addition to MS subtypes that often progresses into another MS subtype (Klineova & Lublin, 2018). Supporting evidence of an MS diagnosis may come from cerebrospinal fluid (CSF) samples with abnormally high immunoglobulins or oligoclonal bands, which are hallmarks of MS (Andersson et al., 1994; Deisenhammer et al., 2019). A better understanding of the disease processes underlying MS may pave the way for more refined diagnostic criteria in the future.

Therapies for MS are often targeted toward the most common subtype, relapsing remitting MS (RRMS). In this form, patients will undergo periods of worsening neurological symptoms followed by remission. Over time, irreversible damage to CNS neurons accumulates and symptoms worsen. A large portion of these patients eventually develop a progressive form of the disease, termed secondary progressive MS (SPMS), characterized by a steady increase in pathology (Kamm et al., 2014). The transition from RRMS to SPMS is still not well understood. In rare cases, the progressive phase begins early in life, before a relapsing-remitting stage is evident, and this subtype is termed primary progressive MS (PPMS).

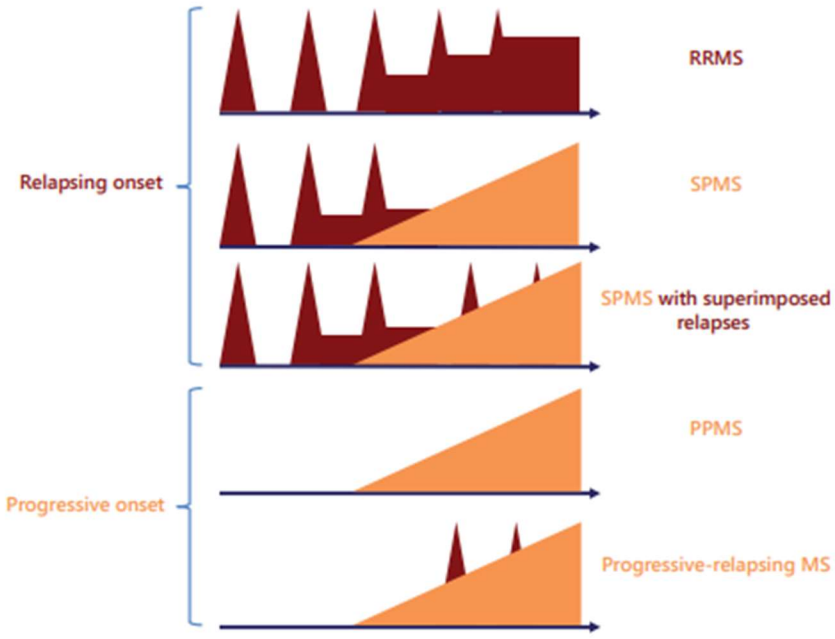

Figure 1: Disease courses in subtypes of MS. Dark red represents areas of relapsing disability, while orange represents progressive increase in disability. The X-axis shows time while Y-axis shows the level of disability. From Kamm et al., 2014.

Treatment options for MS patients are rather limited, and progress developing new options has been slow. The first approved treatment for MS was IFNβ-1b injection, and this was approved specifically for RRMS. Injections for MS treatment were riddled with side effects and lacked promise (Gholamzad et al., 2019). Despite this, it took over a decade for the next type of therapy to be approved: oral medication. These were much more diverse in their mechanism of action compared with injections and are much more tolerable for patients (Goldschmidt & McGinley, 2021). SPMS treatment usually involves disease-modifying drugs (DMDs) that aim to reduce relapses and lengthen

remission periods. However, each of these treatments retain harmful side effects, often those with severe impact on daily life such as bradycardia or liver enzyme elevations. These severe side effects add limitations to how frequently treatment can be administered and come with heavy risk to the patient. Additional therapies target common symptoms of MS such as pain or dizziness, and approved treatments specifically for MS remain largely unavailable. It is apparent that more research must be conducted to identify treatments for MS and each of its subtypes that will treat the roots of the disease rather than the superficial symptoms.

As MS is associated with immune dysfunction, much interest has been placed on discovering the immune cells or processes that may underly MS pathology. In the past, the main immune cell implicated in MS was the T cell. It is thought that T cells, mainly helper T cells (Th cells), are responsible for autoimmune reaction to CNS myelin, causing inflammation and demyelination in the CNS (Segal, 2019). They have also been implicated in the breakdown of the blood-brain barrier (BBB), mainly through the production of interleukin-17 (IL-17) (Huppert et al., 2010), allowing recruited immune cells from the periphery to invade the CNS and add to the damage. Because of their role in MS pathology, Th cells have been the target of drug treatments for MS in a variety of different mechanisms (Kunkl et al., 2020). However, T cells have recently shared some of the research attention with another immune cell: B cells. These cells have several functions in normal immunity, such as antigen presentation and the secretion of cytokines, some of which may be dysregulated in contribution to MS pathology. For example, a subset of B cells was found to have a significantly lower production of IL-10

in MS patients compared to controls (Cencioni et al., 2021). Recently, a breakthrough treatment for MS called ocrelizumab was approved which targets the specific B cell-associated antigen CD20. The DMD uses this antigen to deplete CD20-positive B cells, and it was shown in a clinical trial to significantly slow the progression of PPMS with side effects comparable to placebo (Montalban et al., 2017). Ocrelizumab (under the brand name Ocrevus) is now the only approved treatment for both PPMS and RRMS. Other DMDs are in clinical trials as researchers aim to develop similar treatments that are effective for multiple MS subtypes.

Alternatively, recent clinical trials have been conducted on drugs aimed at slowing or preventing neurodegeneration that may result from prolonged demyelination caused by MS. Among the tested treatments in these trials were the uses of simvastatin and fluoxetine. Simvastatin was shown to significantly reduce the rate of brain atrophy in MS patients compared to placebo (Chataway et al., 2014). Fluoxetine alone could not significantly improve brain atrophy rates in the clinical trial (Chataway et al., 2020). However, fluoxetine has shown promise as a modulator of neurogenesis (see *Drug Treatment*), which may be an important tool for improving MS pathology.

Modelling MS with Lysolecithin

For researchers aiming to study MS, human subjects are most often unavailable or unsuited for the experimental aims. Rodents are a popular model organism for MS as they have well-established backgrounds, and several models exist for studying different

subtypes of the disease. One commonly used method for mimicking MS is the cuprizone-fed model in mice. Mice used in this demyelinating model are fed cuprizone, a copper chelating agent, which is toxic to oligodendrocytes and thus results in widespread demyelination. However, cuprizone has struggled to translate well into rats, as some rat strains have been shown to resist demyelination on a cuprizone diet (Love, 1988). Therefore, the cuprizone model of MS, while advantageous for many applications in mice, would not be suitable for studying MS in rats.

Another popular model that is often used in rats is the lysolecithin demyelination model. In this simplified form of MS, the rodent is injected with lysolecithin in a desired location to induce a focal injury that resembles lesions seen in the brains of human MS patients, and recovery from these injuries can be assessed over time. Lysolecithin integrates into lipid membranes causing membrane disruption which, if applied to myelinated axons, leads to demyelination. Here, we implement the use of lysolecithin injection in rats as a model for MS by targeting the corpus callosum. This white matter tract carries axons from one brain hemisphere to the other, allowing coordination of each side of the body. We target the region of the corpus callosum containing axons from the rat forelimb motor cortex so that these demyelinated axons will have conduction deficits which manifest as motor dysfunction in the animals. Unilateral injury to the corpus callosum has been shown to cause deficits in the limbs ipsilateral and contralateral to the damage in Sprague-Dawley rats (Price and Fowler, 1981), and unilateral damage in the cortex can modulate motor function in in the opposite limb (Allred et al., 2010). Additionally, human MS patients with damage in the corpus callosum display altered

motor cortex activity in the ipsilateral hemisphere indicative of a loss of cross-hemisphere inhibition through the corpus callosum (Lenzi et al., 2007). Thus, it is imperative that the ipsilateral and contralateral limbs are evaluated independently to incorporate these possibilities and to translate the results to humans.

Lysolecithin leads to a profound demyelinated lesion at 4hr after injection that slowly increases in magnitude even at 72hr post injection, and oligodendrocytes are significantly reduced in the lesion area at 24hr post injection (Plemel et al., 2018). Due to the 72hr delay in maximum lesion area, we will assess the motor dysfunction after this window of demyelination to allow time for the injury to fully expand. Much of the functional deficits caused by lysolecithin have been attributed to the demyelination, though some axonal damage has also been shown (Plemel et al., 2018). Lysolecithin provides an excellent MS model as it allows a region-specific demyelinated injury characteristic of MS with precision not offered by other MS rodent models such as cuprizone.

Drug Treatment

In this study, we use a combination of fluoxetine, ibuprofen, and ascorbic acid to rescue behavioral and histological effects of a demyelinating lesion characteristic of MS. These drugs were chosen for their potential to enhance neurogenesis and remyelination. Selective serotonin reuptake inhibitors (SSRIs) such as fluoxetine have been shown to increase neurogenesis in the CNS (Ohira et al 2013), and it is thought that this occurs

through immune modulation. Because MS is an autoimmune disorder primarily affecting middle-aged individuals, it would reason that altering the brain to a phenotype more like that of a younger individual may ameliorate the disease. Fluoxetine has been shown to cause a shift in microglia phenotype from pro-inflammatory (M1) towards anti-inflammatory (M2) (Su et al., 2015). However, this distinction is not binary, as microglia exist along a spectrum of activation from M1 to M2. Generally, M1 microglia secrete pro-inflammatory cytokines such as Il-6 and IL-1β that increase neuroinflammation, while M2 microglia produce the protective cytokines IL-4 and Il-10, among others (Cherry et al., 2014). In an immune model of MS, experimental autoimmune encephalitis (EAE), mouse M2 microglia were shown to be protective through IL-4, as the expression of this cytokine and M2 markers were inversely correlated with the severity of EAE (Ponomarev et al., 2007). Additionally, aging brains have altered microenvironments that favor inflammatory immune phenotypes, such as gene expression patterns and cytokine concentrations (Lee et al., 2000; Frank et al., 2006), and aging itself may have negative consequences on microglia through the accumulation of post-injury effects (Lourbopoulos et al., 2015).

The use of fluoxetine, we believe, allows the brain to be reverse-aged by immune modulation and by increasing the ratio of M2:M1 microglia, thereby allowing neurogenesis to occur more readily through reducing inflammation. Ibuprofen increases plasmin by inhibiting the plasminogen activator inhibitor-1 (PAI-1) (Zapolska-Downar et al., 1999). The increase in plasmin thereby reduces inflammation through the cleavage of fibrin while increasing the cleavage of proBDNF to the mature form of BDNF that aids in the survival of newborn cells (Wang et al, 2021). Ibuprofen also reduces CNS

inflammation through inducing apoptosis in inflammatory activated microglia (Elsisi et al., 2005). Thus, we implement ibuprofen in this study to reduce inflammation that would otherwise interfere with neurogenesis and oligodendrogenesis in the adult neurogenic niche, the subventricular zone (SVZ). Ascorbic acid has been shown to increase myelination in vitro and in vivo through enhancement of oligodendrocyte precursor cell (OPC) differentiation and oligodendrocyte maturation (Guo et al., 2018). Ascorbic acid therefore provides a complementary function to fluoxetine and ibuprofen in this drug combination that promotes remyelination after injury. Increases in neurogenesis and oligodendrogenesis, as well as OPC maturation into oligodendrocytes, promote remyelination after a demyelinating injury, largely through the survival of newborn cells in the SVZ. Previous work by this lab has shown an increase in SVZ neurogenesis with administration of fluoxetine and with fluoxetine, simvastatin, and ascorbic acid combination in healthy animals (Corbett et al., 2015), and this combination also proved efficient at improving injury recovery over time in an endothelin model of stroke. Because of the effects on the SVZ that have been shown by this treatment, it will be of interest to investigate the effects that occur on microglia in this region during this study. Together, we believe the combination of fluoxetine, ibuprofen, and ascorbic acid (FIAA) has the cumulative ability to effectively revert the damaged brain to a phenotype more like a developing brain, promoting neurogenesis and oligodendrogenesis to ameliorate symptoms of MS.

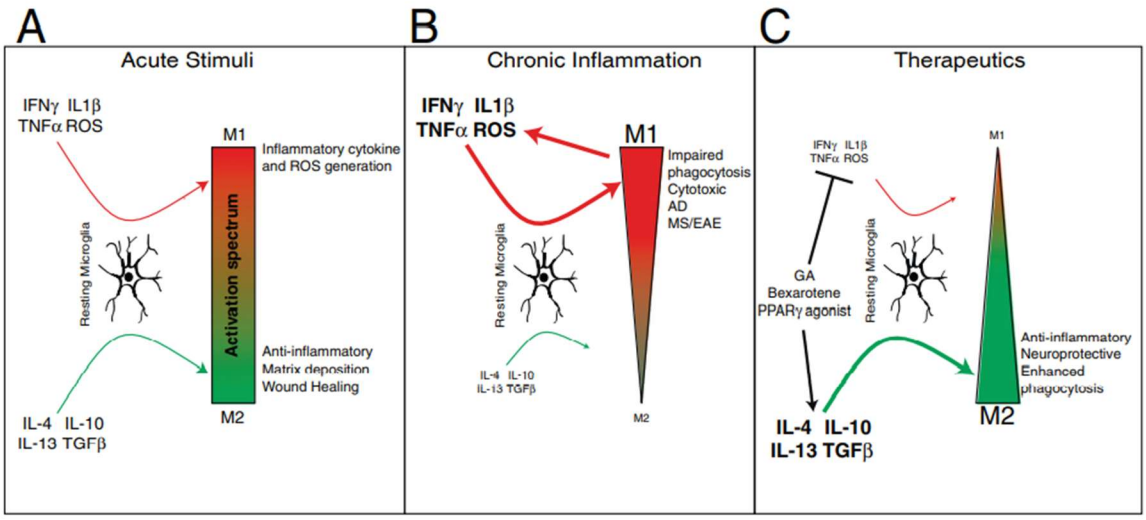

Figure 2. Microglia exist along a spectrum of activity from M1 to M2. Under normal conditions microglia may be activated toward a M1 or M2 phenotype to adapt to the needs of the CNS parenchyma. Chronic inflammatory conditions such as MS shift microglia to a more inflammatory phenotype, while fluoxetine shifts microglia towards M2. Figure from Cherry et al., 2014.

Microglia and the Fractalkine Receptor

Microglia are the resident immune cells of the CNS, comprising an estimated 5-20% of all glial cells in the CNS. First characterized by Pío del Río-Hortega over one hundred years ago, it was long thought that microglia solely performed phagocytosis as the immune regulators of the CNS, and microglia are even considered the brain's tissue-resident macrophage (Prinz & Priller, 2014). In fact, microglia serve a wide variety of roles in the CNS, many of which are non-immune. Apoptotic cells are phagocytosed by microglia during homeostasis, and dendrites and excess synapses are pruned via

microglial phagocytosis during early development (Paolicelli et al., 2011). Microglia serve critical roles in learning and memory, supporting synapse formation via brain-derived neurotrophic factor (BDNF) and neuronal tyrosine kinase B (TrkB) signaling (Parkhurst et al., 2013). Additionally, microglia are responsible for debris clearance during insult or injury (Cignarella et al., 2020) and help recruit additional immune cells from the periphery to facilitate recovery. Inflammatory microglia can activate astrocytes to coordinate astrogliosis and reactions to immune disturbances in the brain (Liddelow et al., 2017). While microglia signal neurons by a variety of cytokines and chemokines such as IL-4 and IL-10, neurons communicate to microglia in part through fractalkine signaling. Existing as the only known member of the CX3C family of chemokines, the fractalkine ligand (CX3CL1) is expressed on the membrane of neurons and is cleaved off for paracrine signaling to the microglial fractalkine receptor (CX3CR1) (Harrison et al., 1998). Binding of the receptor induces an intracellular calcium increase that facilitates the restructuring of microglial actin, thereby causing chemotaxis and microglial migration (Maciejewski-Lenoir et al., 1999; Harrison et al., 1998).

Although widely expressed by immune cells in the periphery (Imai et al., 1997), microglia express CX3CR1 at much higher levels than other cells in the CNS (Maciejewski-Lenoir et al., 1999), making it a useful tool in identifying microglia. Many studies in the past utilized the protein ionized calcium-binding adapter molecule 1 (Iba-1) as a marker of microglia, but it is recently being replaced by CX3CR1 due to studies identifying microglia that lack Iba-1 expression (Waller et al., 2019). The CX3CR1 pathway has also been implicated in modulating neurogenesis. It was found that CX3CR1 are necessary for neurogenesis in the hippocampus, likely through IL-1β, as loss of

function of CX3CR1 significantly reduced signs of hippocampal neurogenesis in aged rats (Bachstetter et al 2011). However, neurogenesis in the SVZ-rostral migratory stream-olfactory bulb pathway does not appear to be affected by changes in CX3CR1 signaling, as CX3CR1 knockout mice displayed no changes in neurogenesis at 2-3 months of age (Reshef et al., 2014). A notable difference between these two findings is the age of the animals (22mo and 2-3mo). This could explain the variability in findings as microglia are known to undergo drastic changes in transcription with age (Gyoneva et al., 2019).

As CX3CR1 signaling leads to reduced microglial activation, it is possible that disturbances in this pathway disrupt neurogenesis through excessive microglial activity such as the secretion of inflammatory cytokines that may be harmful to immature cells (Cardona et al., 2006). Additionally, in the brains of older animals the function of these cells may decline as part of senescence to include reduced neuron-microglia communication that may explain the reduction in neurogenesis with aging. Indeed, adult mice have been shown to express hippocampal CX3CL1 in reduced amounts when compared to young animals (Vukovic et al., 2012). Interestingly, it was also shown that exercise can rescue this effect (Vukovic et al., 2012), hinting at the possibility that the reduction may be a result of the decline in activity with age rather than an unavoidable cellular degradation. Additionally, a recent study demonstrated the importance of CX3CR1 in maintaining a young-brain microglial profile: It was found that the transcriptome of microglia from young mice can be made more like that of aged mice by genetic knockout of CX3CR1 (Gyoneva et al., 2019). Declines in both ligand and receptor due to aging point to the fractalkine system as a critical mediator of microglial activity that may provide therapeutic benefits in microglia-related diseases where age is

an important risk factor. In the present study, we use CX3CR1 as a marker for microglia and examine their distribution in a model of neurogenesis and oligodendrogenesis in the SVZ following demyelination by lysolecithin.

II. METHODS

Animal Husbandry

All animal treatments were approved by the Wright State University IACUC board before proceeding. To mirror the age and sex bias of MS, thirty female Sprague-Dawley rats were acquired as retired breeders, aged 10-11 months. The rats were given a three-day acclimation period to adjust to the new housing environment. Rats were kept one per cage with adequate room for mobility. Bedding was a combination of wood chips and paper shredding, along with a cardboard tube for anxietolytic isolation. All animals were kept in the same room to control for temperature, humidity, and lighting conditions. Temperature control was fixed at 74°F. Animals were kept on a 12hr light-dark cycle, which remained consistent throughout the experiment. Animals were fed ad libitum rat chow except during times of dietary restriction for Montoya staircase testing. Water bottles were provided ad libitum throughout the entire experiment.

Montoya Staircase Test

Middle-aged (10-11 months) female Sprague-Dawley rats (n=30) were trained on an improved Montoya Staircase test (Montoya et al., 1991) which included a color-coding method for identifying pellet drops: Each well contained three banana-flavored

pellets dyed with a color unique to that well. It could thus be determined from which well a dropped pellet originated. Rats were acquainted with the training environment for several days before training began. Staircase training occurred twice per day, once in the light cycle and once in the dark cycle, for two weeks. During training, animals are placed into the staircase apparatus and encouraged to take pellets by the experimenters through visual and auditory cues. Animals were considered properly trained if they successfully took 9 pellets per paw in a training session. Of the 30 animals trained, 27 (90%) successfully learned the task before surgery. Animal *ad libitum* food intakes were measured during the acclimation period, and rats were fed at a slight (15%) deprivation from these amounts to encourage taking pellets. During scoring sessions, rats were placed into the staircase apparatus during the dark cycle and given 15 minutes to take pellets. The rats were then returned to their cages and the remaining pellets were counted. Animals were scored based on pellets eaten, dropped, and their accuracy for pellet retrieval (Kloth et al., 2006). Pellets that were located outside of their original well are deemed dropped, while pellets missing or behind the differentiator are deemed taken (see Figure 3). Five rats were scored in each 15-minute session. Post-surgery scoring occurred in groups of three-day time points, beginning on post-surgery days 3, 15, 30, and 45, and scores were averaged among each of these three-day time points. Pellets were refilled after each scoring session. Individual rats used the same apparatus on every scoring day, and the staircases were cleaned after each session to mitigate distracting odors. An animal's score on the staircase test is used as a representation of the functional capabilities of the forelimb tested

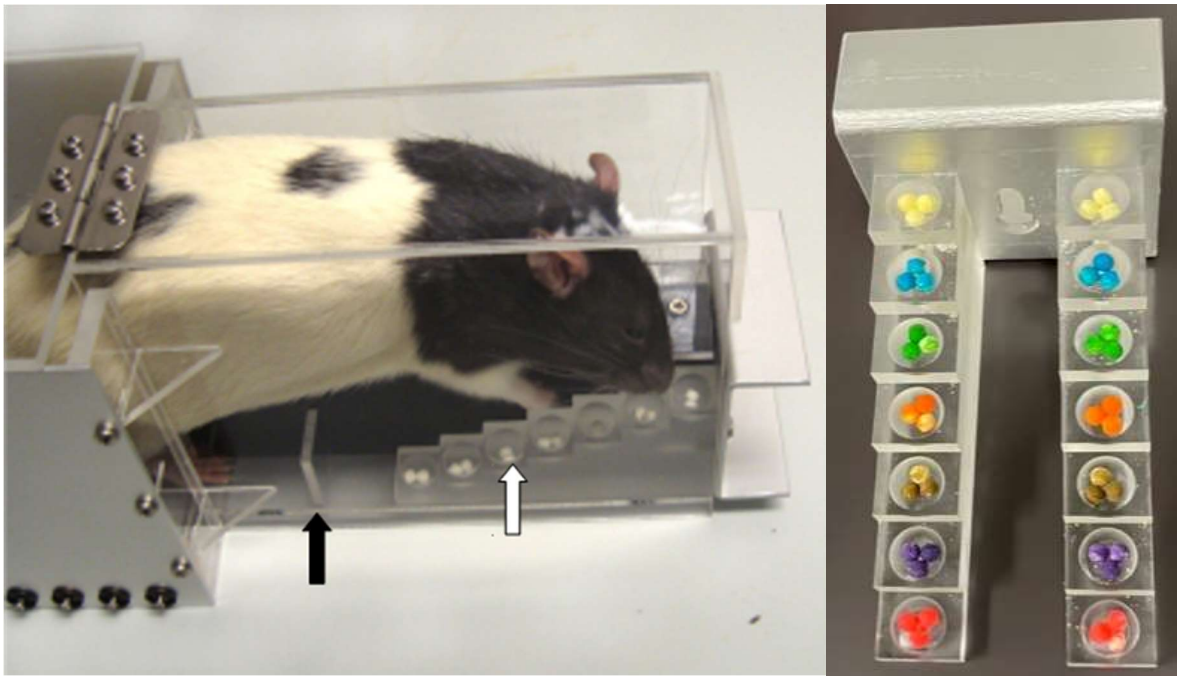

Figure 3: Example of Montoya staircase test apparatus. **A.** The rat lies on an elevated platform and must extend their forepaws to reach for sugar pellets in wells of various heights. Grasping ability is measured by pellets dropped relative to pellets taken. **B.** In our studies, seven levels of wells were used, each with uniquely colored pellets. White arrow indicates one well. Black arrow indicates dropped/taken differentiator. Figure in panel A modified from Wang et al., 2011.

Drug Treatment Regimen

Animals were given either vehicle or FIAA treatment in vehicle once daily for 40 days beginning six days post-surgery (after initial functional deficit could be established in post-surgery days 3-5), so that the last day of drug treatment was the final day of Montoya staircase testing. Fluoxetine (5mg/kg), ibuprofen (20mg/kg), and ascorbic acid

(50mg/kg) were administered together using voluntary oral administration with a sugar cookie dough vehicle to minimize stress (Corbett et al., 2012). Drug intake was confirmed by observation of cookie dough absence typically within five minutes. This method of drug administration is critical as stress is a known correlate with MS pathology and decrease of neurogenesis. Table 1 (below) shows the breakdown of the 30 animals and which treatment they received.

Group	**# of Animals**
Control	14
Sham Control	1
FIAA	13
Sham FIAA	2
Total	**30**

Lysolecithin Surgery

To induce focal demyelination, lysolecithin was injected into the brain of each animal following initial Montoya staircase training. Animals were anesthetized by 5% isoflurane prior to surgery. When fully anesthetized (~5 minutes), the animals' head was quickly shaved, and they were immediately moved from the isoflurane chamber into the stereotaxic apparatus. Continuous anesthesia by 2.5% isoflurane was given during surgery with 0.6L/min of oxygen delivery. The animal was held in the stereotaxic apparatus via bite bar and ear bars as well as a surgical glove tied around the chin for added support. The animals' eyes were lubricated with eye lube to prevent dryness during

anesthesia. After administration of bupivacaine at the surgical site, a small midsagittal incision was made from the eyes to about the midpoint between bregma and lambda, exposing bregma. A micro-drill was then used to bore three holes for needle puncture at the following coordinates: anterior posterior (AP) 0mm, mediolateral (ML) -2.5mm; AP 1.5mm, ML -2.5mm; AP 3mm, ML -2.5mm. The coordinates for injection were selected to target the right corpus callosum containing axons from the forelimb motor cortex. A syringe was then inserted into the holes at a depth of 2.9mm and 2μL of 1% lysolecithin in phosphate-buffered solution (PBS) was injected over the course of several minutes in small increments. Once finished, the syringe was slowly retracted from the animal. The incision was then sutured shut and dotted with iodine, and the anesthesia was stopped. Animals were moved to a warming bed for recovery and given 200mg/kg of acetaminophen per day for three days post-surgery. All surgeries were performed using aseptic techniques with autoclaved instruments. The resulting injury can be seen in Figure 5 in the Results section.

Tissue Collection and Processing

Following the final day of drug treatment and Montoya staircase scoring, the animals were sacrificed for tissue collection. In preparation, animals were injected intraperitoneally with neutral red dye prior to euthanasia for post-mortem visualization of the injury site. Animals received an intraperitoneal injection of pentobarbital (Euthasol) before cardio perfusion with PBS followed by paraformaldehyde (PFA): PBS is flushed through the body to remove blood from the animal, while PFA is used to fix the tissue.

The rats were then decapitated, and the brains were removed. The cerebellum and olfactory bulbs were removed, and the rest of the brain was cleaned of any excess tissue and placed into PFA solution. The solution of PFA was later poured off and replaced by 30% w/w sucrose for at least three days. For cryosectioning, a light coat of optimal cutting temperature (OCT) compound was dripped onto the cryostat chuck. The sucrose solution is then poured off and the sample is placed onto the chuck, then covered with OCT compound. Covered samples are then placed into the cooling chamber for approximately 30 minutes to freeze at -23°C. Chucks were then moved to the sectioning mount and brains were trimmed to the beginning of the ventricles. The brains were then sliced into 50μm coronal sections to be collected. Slices were placed into vials of PBS solution to prepare for antibody staining.

Immunohistochemistry

All immunohistochemical procedures were performed on a rocking plate to ensure homogenization of solutions surrounding brain slices. To begin, PBS solution was removed from section-containing vials and sections were incubated in several drops (enough to cover the sections) of Bloxall for 10 minutes. Bloxall was then removed and replaced with blocking solution of PBS tween with 3% goat serum and incubated for one hour. After incubation, the primary antibody was added and incubated for 30 minutes, then removed and sections were washed with 3mLs of PBS tween. Blocking solution was again added and the secondary antibodies were allowed to incubate in the solution for 30 minutes. Slices were washed with PBS tween followed by incubation in

avidin/biotinylated enzyme complex (ABC) solution for 30 minutes. After a final wash, DAB was added to the slices for 10 minutes before promptly removing and replacing the solution with distilled water. Stained slices were then mounted onto gel-coated slides with a fine-tipped paint brush. Once dry, slides were coated in DPX mountant and covered with a glass coverslip.

Imaging and Quantification

Digital images of brain slices were captured under 40X total magnification (10X objective, 4X ocular) in a confocal microscope. Ventricles were often too large to capture in one image under this magnification. In these cases, several pictures were taken and stitched together in Adobe Photoshop. Images are then converted to binary 8-bit black and white images for analysis. Representative masks of CX3CR1 staining were created and quantified using ImageJ software by changing the black/white threshold. The level was adjusted until only the ventricular staining was present and background staining was eliminated. Eliminating background staining allowed labeling to be measured with normalization to the brightness of the total slice. The same criteria were used for eliminating background staining in the whole ventricle measurements and the corpus callosum measurements. Thus, some corpus callosum slices yielded staining values of zero.

Whole ventricle quantification included outlining the ventricle using the freehand tool in ImageJ before adjusting threshold. A trace was made slightly outward of the ventricle border to capture staining on the ventricle border. For corpus callosum quantification, only the staining adjacent to the corpus callosum was selected using the freehand tool. The corpus callosum was delineated first by identification of the dorsal ventricle border. Then, a trace was made until the apex of the medial and lateral curves on either side of the dorsal border. The scale was set to 980.71 pixels/mm, determined by a 1mm scale bar image taken with the same microscope under the same magnification. Staining was then converted to pixel masks and the total area of the masks was measured.

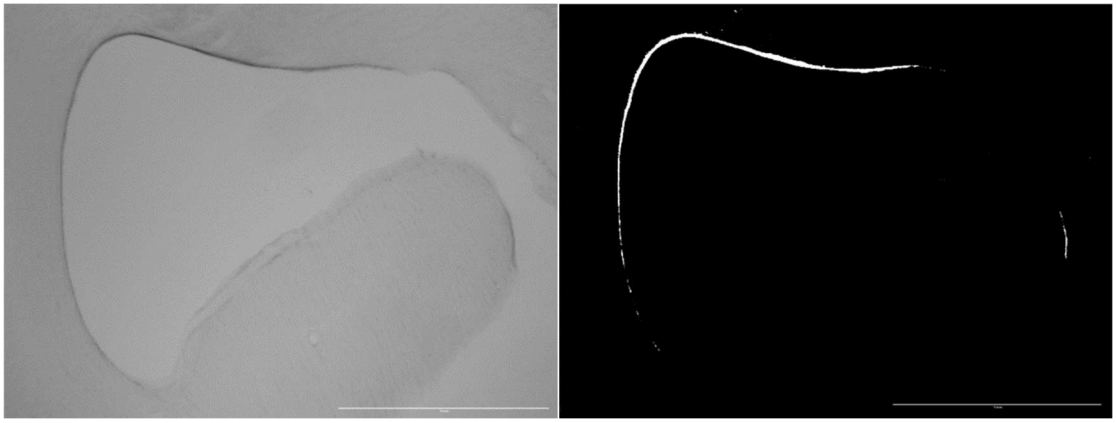

Figure 4: Representative posterior ventricle coronal section (left) stained for CX3CR1 along with quantitative mask (right). Ventricle is oriented with dorsal to the left. CX3CR1 staining is observed along the corpus callosum and on the lateral side of the ventricle. Mask was produced using ImageJ by adjusting the threshold to only show labeled area and limit background staining. Scale bar is 1mm.

Statistical Analysis

The total CX3CR1 staining area was collected for each section as described above. Section staining is then determined for each animal, separated by region of the ventricle and by experimental group. The regions were divided into anterior, middle, or posterior. Experimental group designation was either control or FIAA treatment group. For each animal, staining was averaged for each area and treatment group. Averages were then entered into SigmaPlot software for analysis. Two-way analysis of variance (ANoVA) with Bonferroni t-test was done to determine statistical differences in staining between regions and experimental groups. Groups were significantly different if $p<0.05$. Outliers in were designated by SigmaPlot as existing below the 5^{th} or above the 95^{th} percentiles. Because no differences were found between experimental and control groups, further analysis of regional differences included grouping all slices by region, regardless of the experimental group. Table 2 (below) depicts the animals from the "Learner" Montoya Staircase group (see table 3) from which staining data was collected and analyzed. Note that several animals which were included in the Montoya Staircase data collection could not be analyzed for CX3CR1 staining due to fixation complications, therefore there are less subjects here than in the functional analysis. Non-learner animals were not included in staircase data collection or CX3CR1 staining data collection.

Group	Animals
Control	12
Treatment	10
Total	**22**

Staircase scores are calculated as average pellets eaten during a 3-day session. Sessions were defined as the following days: pre-surgery, post-surgery days 3-5, post-surgery days 15-17, post-surgery days 30-32, and post-surgery days 45-47. These are then divided by the average pre-surgery scores for that animal to normalize forelimb function across the group. Scores on the staircase test are used to measure forelimb function as a quotient of post- and pre-surgery. An example of this is as follows:

$$Function = \frac{Average\ pellets\ eaten\ in\ specified\ session}{Average\ pellets\ eaten\ per\ session\ pre-surgery}$$

To evaluate differences in function, scores are sometimes referenced in terms of score decreases, or deficits. This is used to compare forelimb function after surgery with pre-surgery, or to compare two scoring days in which forelimb function has decreased. An example of this calculation is shown below:

$$Functional\ Deficit = Function\ before\ surgery - Function\ on\ day\ X$$

Scores were also evaluated as recovery from the deficit. This was determined to be the increase in pellets taken on the final 3-day session (post-surgery day 45-47) when compared to the initial deficit (post-surgery days 3-5). An example of the calculation used to find recovery is shown below:

$$Functional\ Recovery = Function\ on\ PSD\ 45 - Function\ on\ PSD\ 3$$

We also assessed the accuracy of the animals. Accuracy was defined as the animals ability to obtain pellets they attempted to reach. Attempts were determined by the number of pellets eaten and the number of pellets dropped. Repeated measures ANoVA were used to determine any statistically significant differences. Accuracy is expressed as a percentage and the calculation is shown below:

$$\%Accuracy = \frac{Pellets\ eaten}{Pellets\ eaten + pellets\ dropped}$$

Outliers in Montoya staircase tests were designated by SigmaPlot as existing below the 5^{th} or above the 95^{th} percentiles. Apparent outliers in correlations were removed and the data retested to determine effects on the R value. Those with dramatic changes to R were excluded as outliers while those with minimal effects were included.

III. RESULTS

The aim of this study was to improve functional recovery following an induced focal demyelinating lesion as evaluated by the Montoya staircase test and identify any possible relationships with microglia and functional recovery. Comparisons in forelimb function (ipsilateral and contralateral separate) between pre- and post-lysolecithin injection are made to determine both initial functional deficit and functional recovery in both controls and treatment groups. The administered drug treatment is a combination of fluoxetine, ibuprofen, and ascorbic acid (FIAA).

It is critical to the experiment that we induce the demyelinating lesion in the correct location. Therefore, histological evidence of the lesion must be obtained in support of the behavioral manifestations we observe here. We attempted to implement the injection of neutral red dye prior to euthanasia as a means of visualizing the lesioned area, but obvious stained areas were not present in sectioned tissues. Therefore, we must rely on other histological support, such as antibodies against microglia which migrate to injury sites. Although CX3CR1-stained sections cannot provide evidence of injury, other antibodies used in the experiment support a corpus callosum injury. Microglia were stained, using methods like those described for CX3CR1 previously, using CD11c and Iba1 antibodies. Evidence of an injury to the corpus callosum comes from the resulting sections obtained using these antibodies as shown in Figure 5. Support for a correct injection site is gathered from the observation of the needle injection path shown in

Figure 5 that terminates directly superior to the corpus callosum, as intended. This is evident with both Iba1 and CD11c antibody stains, (A-B and C-D, respectively). The high density of CD11c staining near the injury site further indicates demyelination has occurred, as CD11c+ microglia have been shown to be important for initial myelination in development (Wlodarczyk et al., 2017), and they have been identified in the corpus callosum in several models of MS (Benmamar-Badel et al., 2020). Absence of this injury pattern on the left ventricles (Figure 5A) confirms the damage is a result of lysolecithin injection and not of treatment.

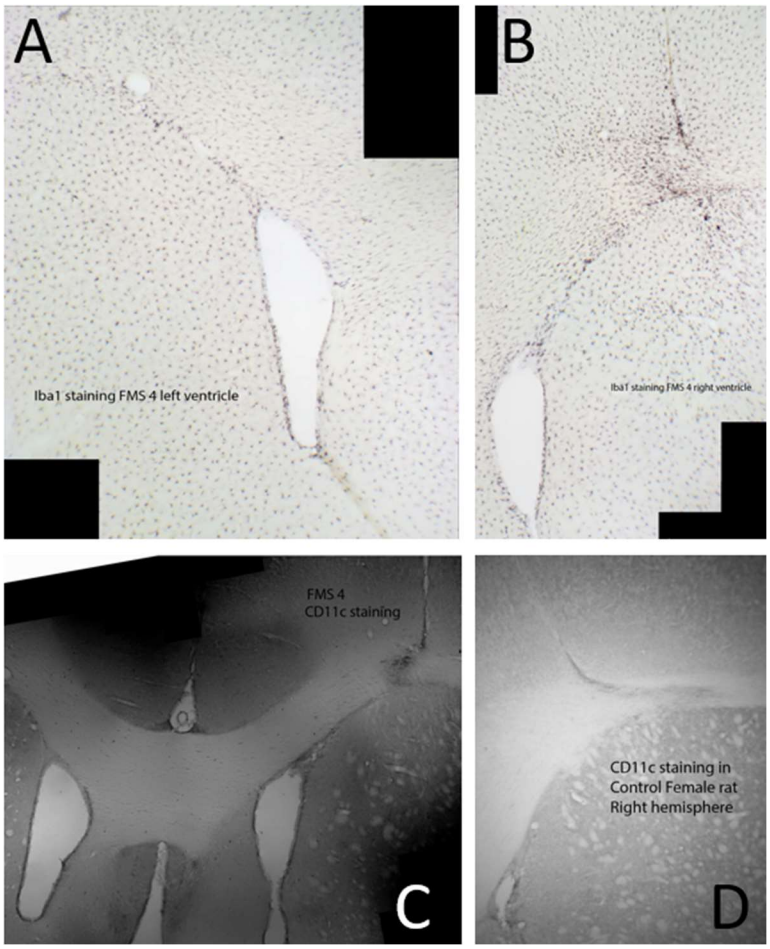

Figure 5: Microglia clustering and the location of the syringe damage support a demyelinating injury in the corpus callosum. Images of coronal sections obtained from

control (D) and FIAA-treated (A-C) animals used in these experiments show microglia stained with either Iba1 (A-B) or CD11c (C-D). Syringe damage is apparent through the cortex and into the corpus callosum of right ventricles (B-D) (vertical line), but absent in the left ventricle which was not injured (A). Microglial staining is darkened slightly inferior to the needle damage and in the corpus callosum near the injury site. Images taken at 40X total magnification (4X objective, 10X ocular), and scaling is the same as shown in figure 4.

Microglia

Staining of CX3CR1 was used to quantify microglia in the lateral ventricles. To account for possible differences arising from proximity to the injury, CX3CR1 staining was divided into anterior, middle, and posterior regions of the ventricles and differences in expression were evaluated for each area (Figure 5). Expression in the posterior region was significantly greater than that of the anterior ($p=0.005$) but not the middle (0.0495 mm^2 vs 0.0472 mm^2) region. Additionally, staining in the middle region was significantly greater than that of the anterior region ($p=0.011$). Statistical tests are pairwise multiple comparison procedures using Bonferroni t-test. Least square means are used for direct comparisons.

Comparison of CX3CR1 expression in the whole ventricle is also divided by treatment: control versus FIAA treatment (Figure 5). The expression was found to be similar in animals treated with control and those with the FIAA treatment ($p=0.517$). There also appears to be no significant interaction between region and drug treatment ($p=0.564$). As several outliers were identified in the analysis (see *Statistical Analysis*), the

tests were repeated with their exclusion to identify any possible impact they may have. Without the outliers, similar results were obtained as before. Posterior staining was found to be significantly greater than that of the anterior region (p=0.005), but not significantly different from the middle region (p=1.000). The middle region displayed significantly greater staining than the anterior region (p=0.010).

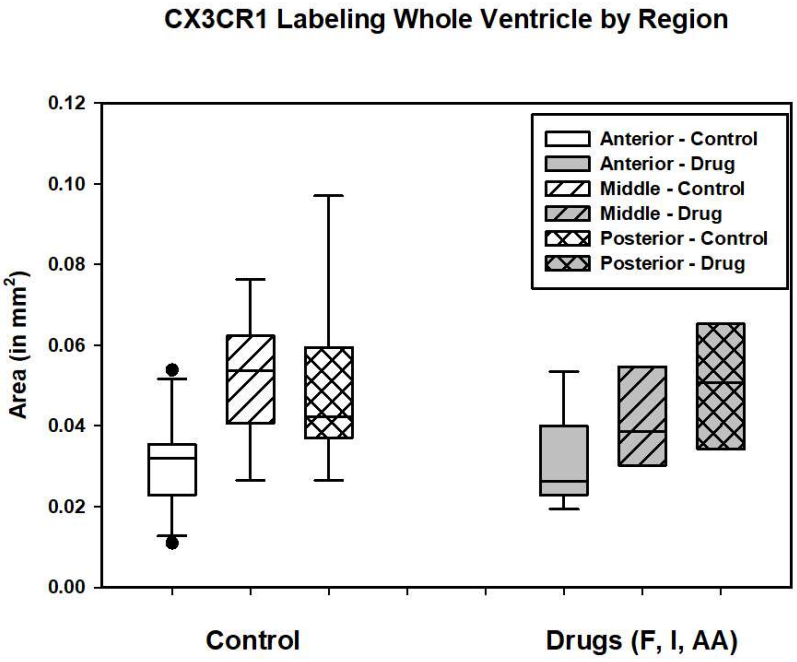

Figure 6: CX3CR1 labeling differs by region in the lateral ventricles of middle-aged female Sprague-Dawley rats. The X-axis shows the experimental group (control vs FIAA) and region (anterior, middle, posterior). The Y-axis shows the labeling area in mm^2. Filled circles represent outliers. Two-way ANOVA was used to identify statistical differences. Box plot produced using SigmaPlot.

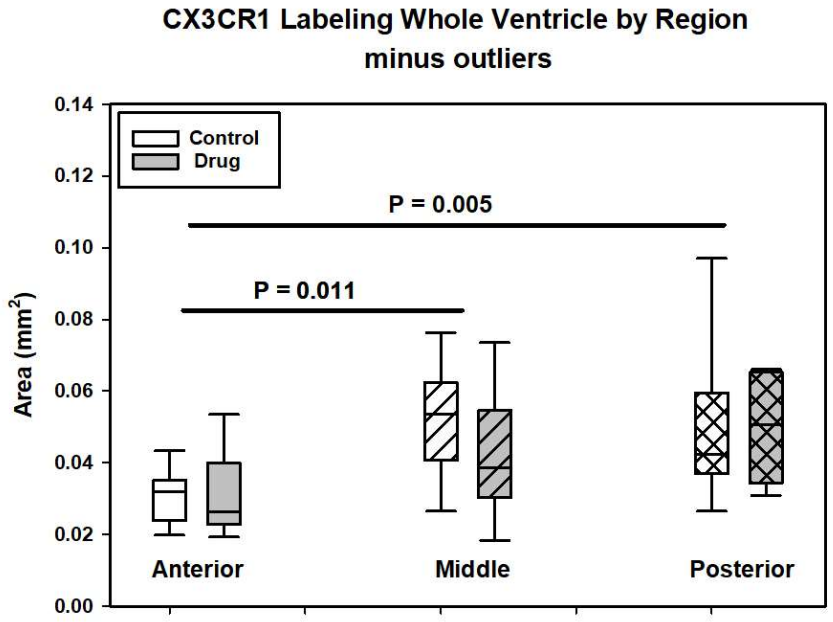

Figure 7**:** CX3CR1 staining in the rat ventricle differs by region. The X-axis shows the experimental group (control vs FIAA) and region (anterior, middle, posterior). The Y-axis shows the labeling area in mm^2. Here, outliers have been removed and the data retested for statistical significance using two-way ANOVA. Box plot produced using SigmaPlot.

Because demyelination largely targets white matter tracts in the brain, and the corpus callosum is largely affected in lysolecithin-injected rats, we evaluated the expression of CX3CR1 in the dorsal border of the ventricles, adjacent to the corpus callosum (Figure 7). As before, the ventricle slices are divided into anterior, middle, and posterior regions to isolate the staining in each. Posterior slices showed greater staining than anterior ($p<0.001$) and middle ($p=0.030$) regions. However, staining was not

significantly different between middle and anterior regions (0.00883 mm^2 vs 0.00466 mm^2, p=0.269). Staining was also not significantly different between treatment groups (p=0.833).

As several outliers were identified in corpus callosum-adjacent ventricle staining (see *Statistical Analysis*), the tests were repeated excluding outliers (Figure 8). Posterior staining remained significantly greater than anterior (p<0.001) and middle (p=0.033) regions, while staining in the middle and anterior regions were not significantly different (p=0.347).

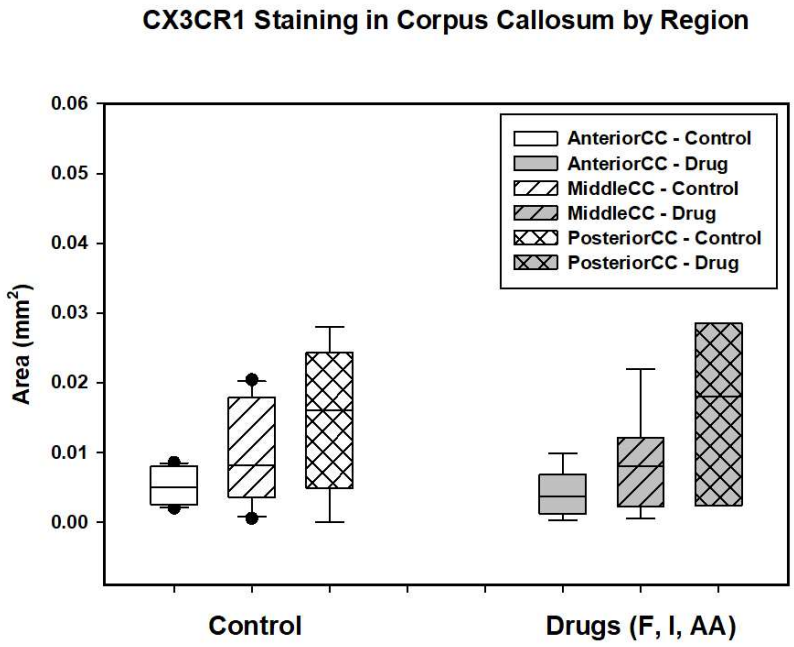

Figure 8: CX3CR1 staining differs by region in the corpus callosum adjacent to the lateral ventricles. The X-axis shows the experimental group (control vs FIAA) and region (anterior, middle, posterior). The Y-axis shows the labeling area in mm^2. Filled circles represent outliers. Two-way ANOVA was used to identify statistical differences. Box plot produced using SigmaPlot.

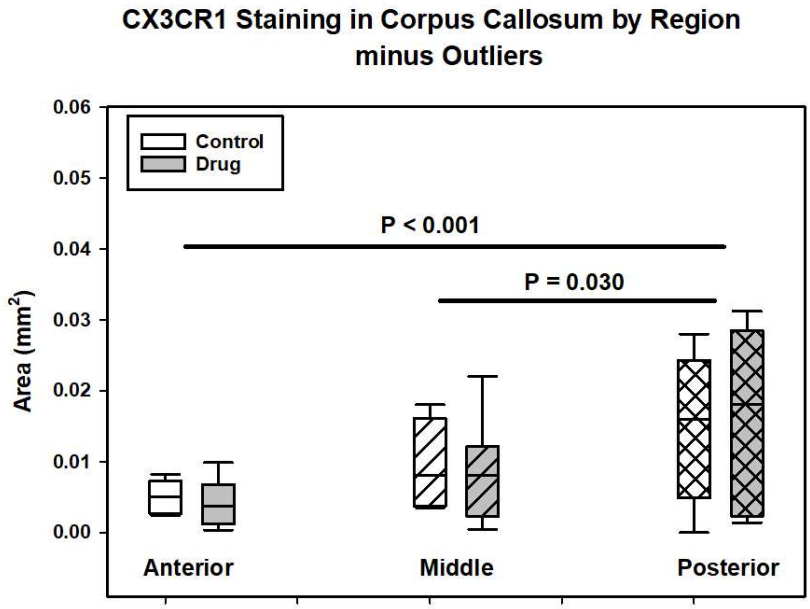

Figure 9: CX3CR1 staining in the corpus callosum differs by region. The X-axis denotes experimental group and ventricle region while the Y-axis denotes the CX3CR1 staining area in mm^2. Here, the outliers have been removed and retested for statistical significance using two-way ANOVA. Box plot produced using SigmaPlot.

Montoya Staircase

The Montoya staircase test was used to measure contralateral and ipsilateral forelimb function before and after the induction of a demyelinating lesion. Contralateral function is used to indicate function in the forelimb motor cortex, and a deficit in contralateral forelimb function is an indication of damage to this region. Ipsilateral function is used to measure function of the corpus callosum, and damage in this area has been shown to result in ipsilateral forelimb functional deficits in Sprague-Dawley rats

(Price and Fowler, 1981). Due to the nature of the Montoya staircase test, each paw can be tested simultaneously, eliminating possible confounding variables by keeping the testing conditions identical. We utilized the Montoya staircase test to measure contralateral and ipsilateral forelimb function to assess recovery from induced focal demyelination. Of the animals trained on the test, 10% were unable to learn and therefore were excluded from the study (see Methods section; see Table 3).

Table 3	# of Animals	% of Animals
Learners	27	90%
Non-Learners	3	10%
Total	**30**	**100%**

Function

Montoya staircase scores were evaluated on the quantity of pellets eaten. Scores were normalized to pre-surgery for each animal to emulate clinical tests of motor function. Learner rats (n=27) were divided between control (n=14) and animals treated with FIAA combination (n=13), and both saw initial deficits (post-surgery days 3-5) in ipsilateral forelimb function after lysolecithin injection. Control animals had an average deficit of 10.4%, while the FIAA treated animals had an average deficit of 6.1%. Control animals improved their scores by post-surgery day 15 with an average deficit of 5.4%. FIAA treated animals had lower scores on day 15 when compared to day 3 (18% vs 10.4%) and when compared to controls, though neither were statistically significant. By post-surgery day 30, controls had fully returned to pre-surgery function with a slightly

improved average score of 101.3% of pre-surgery, and this improvement was sustained through day 45 with an average score of 101.7% of pre-surgery. Meanwhile, FIAA treated animals never fully recovered from the injury. These animals saw a functional deficit of 12.5% on post-surgery day 30 and a similar trend on day 45 with a deficit of 10.5%. Overall, there was no statistically significant difference between controls and FIAA treated animals. There also was no statistically significant difference in scores over time.

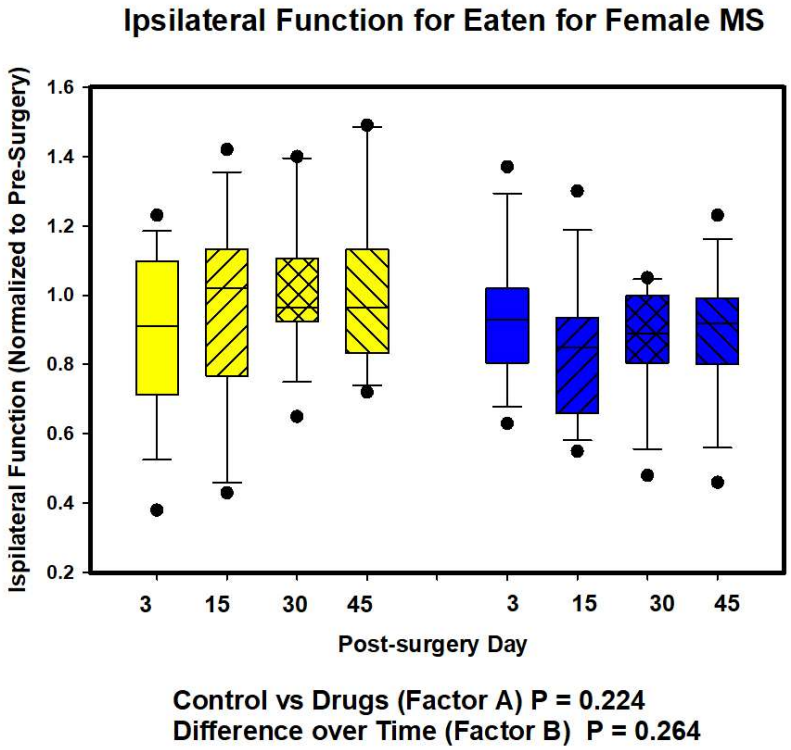

Figure 10: Ipsilateral function was affected by lysolecithin injection to a lesser extent than contralateral function and exhibited no significant recovery over time. Yellow bars (left group) represent controls while blue bars (right group) represent treated animals. The Y-axis shows function of the ipsilateral limb measured by pellets eaten normalized to pre-surgery function. The X-axis depicts the day post-surgery on which the

measurements were taken. The maximum, 25th percentile, median, 75th percentile, and minimum are shown for each box, with outliers represented as filled circles. Controls and drug treatment animals displayed similar results. Neither controls nor drug treatment animals recovered significantly over time. Statistical measurements were repeated measures ANoVA.

Like ipsilateral forelimb function, contralateral function was also decreased in controls and FIAA treated animals following lysolecithin injection surgery. However, the initial deficits were much larger for contralateral forelimbs. Controls saw an average deficit of 38.4% (61.6% of initial function) on post-surgery day 3, and FIAA treated animals had an average of 39.2% functional deficit (60.8% function compared to pre-surgery). Control animals then showed improvement on day 15 with 83.9% of their pre-surgery function returned and recovered full function on day 30 with scores of 101.6% compared to pre-surgery. On day 45 the control animals saw no further improvement and had an average function of 98% that of pre-surgery.

After the initial deficit, FIAA-treated animals showed a slight improvement in contralateral forelimb function with an average 64.2% function on day 15 compared to pre-surgery. These animals then held a steady increase in contralateral function with 77.5% function on day 30 and 84.5% on day 45, though these changes were not statistically significant.

Overall, contralateral function saw a near significant difference between controls and FIAA treated animals ($p=0.074$). The animals as a group saw a significant improvement in contralateral function over time ($p<0.001$). The most significantly

different days were post-surgery days 45 and 3 ($p<0.001$) and post-surgery days 30 and 3 ($p<0.001$). There was also a statistically significant increase from day 15 to day 45 ($p=0.030$).

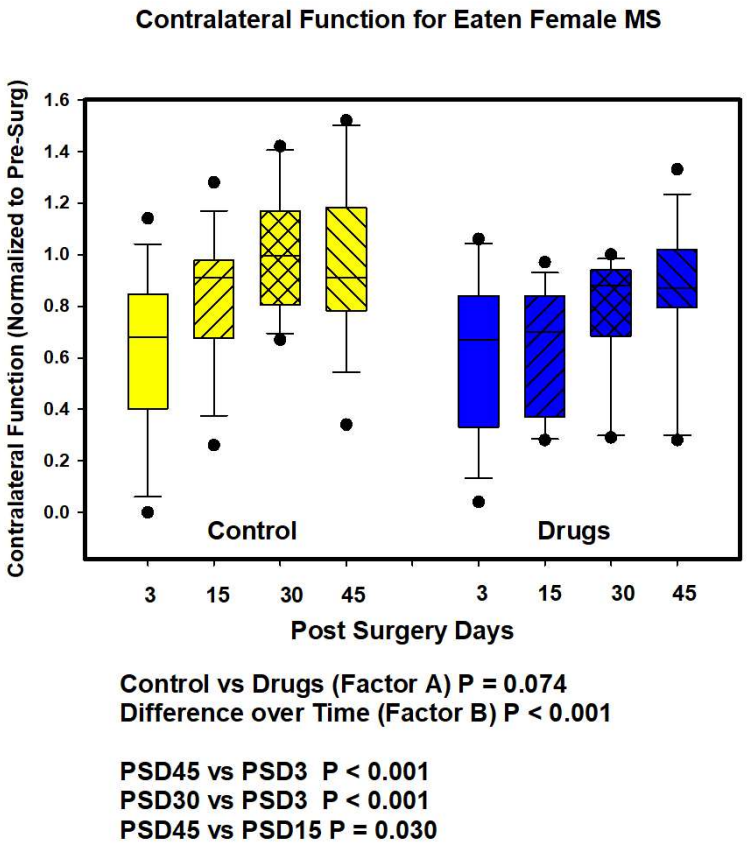

Figure 11: Contralateral forelimb function was adversely affected more by lysolecithin injection than ipsilateral forelimb function, and animals recovered significantly over time. The Y-axis shows function of the ipsilateral limb measured by pellets eaten normalized to pre-surgery function. The X-axis depicts the day post-surgery on which the measurements were taken. Control and drug treated animals performed differently, though only nearly statistically significant. Contralateral function clearly recovered over

time, with significant differences at several post-surgery time points. Statistical tests are two-way repeated measures ANoVA.

Accuracy

To further determine the performance of animals on the staircase test, the animals were also evaluated based on their accuracy (or success rate) of retrieving pellets. Accuracy includes the pellets dropped and eaten by the animal and scores them based on pellets eaten over the total pellets attempted (see Methods). This measure incorporates dropped pellets into the analysis, unlike function described previously. We predicted that animals in the FIAA treatment group would have significantly lower accuracy during later time points when compared to controls. Additionally, animals would exhibit poor success rates immediately after the injury due to loss of motor function, and this was expected to recover over time as did function.

When we analyzed the accuracy of the animals' contralateral limb, we did not observe any apparent drug effects ($p=0.946$). We did however find additional evidence of the large cortical injury, as the animals' accuracy was significantly reduced after the injury when compared to pre-injury (84.5% before injury, 74.9% after injury; $p=0.006$ for combined samples). This indicates that lysolecithin damage to the cortex interfered with the animals' ability to grasp pellets with their contralateral forelimb. Both the control and FIAA treated groups displayed significant recovery over time, improving their accuracy over the course of the experiment ($p=0.002$). Animals successfully recovered back to pre-surgery accuracy, as post-surgery day 45 and pre-surgery accuracy were identical ($p=1.000$). Nearly all the recovery in accuracy appeared to be focused in the days

between post-surgery day 3 and post-surgery day 15, as the accuracy was significantly increased on day 15 compared to day 3 (83.7% vs 74.9%; p=0.015), but day 30 and day 45 were not significantly different from day 15 (p=1.000 for each). The increases in accuracy are most likely due to the recovery from injury that improves the animals motor function back to pre-injury performance.

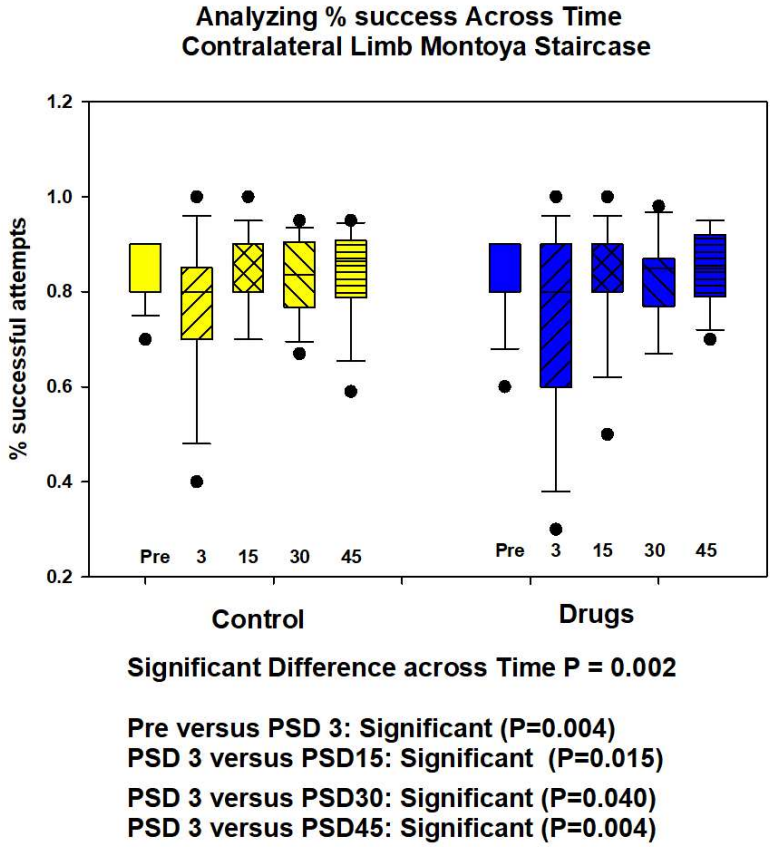

Figure 12: Accuracy of acquiring pellets attempted on the Montoya Staircase test returns to baseline after recovery from injury. Animals were evaluated on their percent success rate (accuracy) of acquiring pellets they attempted to reach. The X-axis separates the data by the 3-day session in which the tests were performed, denoted by the day the session began, as well as by treatment received (control or drugs). The Y-axis represents the accuracy of the animals in decimal form, with 1.0 being a perfect accuracy (no dropped

pellets). Filled circles represent outliers. Two-way repeated measures ANoVA was used to test for statistically significant differences.

Correlations

We next wanted to investigate any possible correlations between functional recovery and the area of CX3CR1 staining. Because there were apparent differences in CX3CR1 staining between regions of the ventricle along the anterior-posterior axis, we predicted that there would also be distinct differences in correlations between functional recovery and microglia in each region. Staining remained divided between anterior, middle, and posterior coronal sections of the ventricles. These were then plotted against functional recovery for each animal, and a trendline was made with a correlation coefficient to identify any relationships. Animals were only included in the correlations if they had sufficient initial functional deficits (predetermined 20% or greater based on prior observation), as determined by Montoya Staircase performance, to mitigate injury discrepancies. Because most animals did not meet the 20% deficit criteria in the ipsilateral limb, correlations were only performed for the contralateral limb.

The control animals showed a moderate positive correlation between their functional recovery and anterior ventricular CX3CR1 staining area, with a coefficient of 0.477, though this was not statistically significant ($p=0.232$). For FIAA-treated animals however, there was a weak negative correlation that was also not significant ($R=-0.353$; $p=0.492$). Therefore, there is no relationship between microglia area in the anterior

ventricle and functional recovery in treated animals, but controls did seem to exhibit a relationship. The relationship in controls is further supported when an identified outlier was removed. This animal had a functional recovery of 140%, well above that of any other animal in the control group, and it was therefore excluded from a follow-up correlation. Correlation of control animals functional recovery and microglia staining in the anterior ventricle without this outlier showed a strong positive correlation with statistical significance (R=0.858; p=0.0135). Therefore, there is a strong relationship between anterior ventricle CX3CR1 staining area and functional recovery in the contralateral limb that is present in control animals and not observed in FIAA-treated animals.

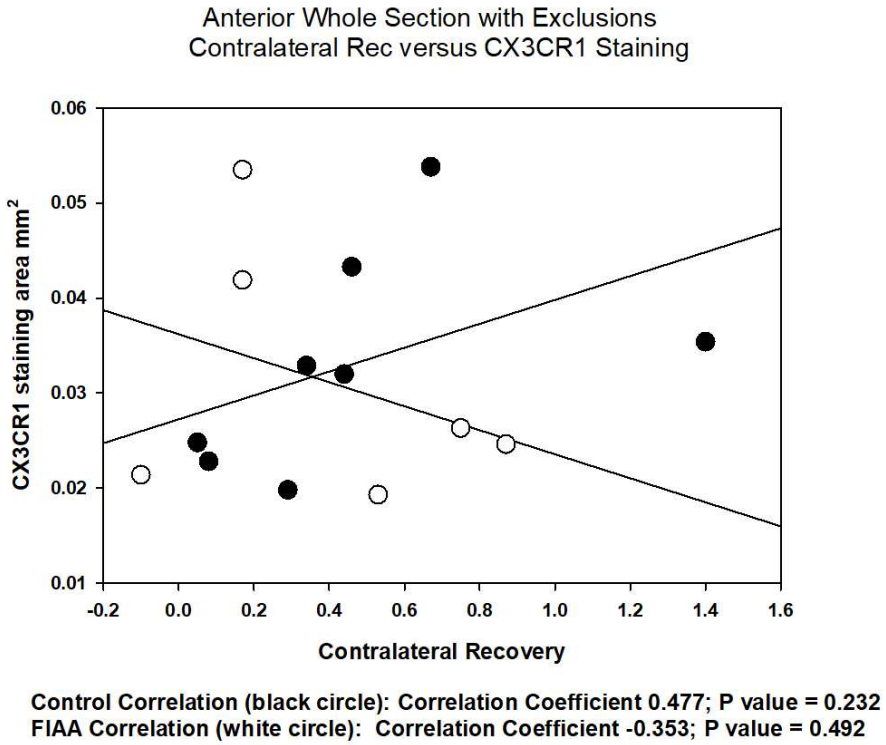

Figure 13: Control and treated animal contralateral functional recovery is not correlated with microglia in the anterior ventricle. The X-axis discerns functional recovery in the

forelimb contralateral to injury, while the Y-axis is CX3CR1 staining area to measure the amounts of microglia. Each filled circle represents one control animal (n=8) while each empty circle is a FIAA-treated animal (n=6). Correlations were only performed on animals which showed sufficient initial deficits of 20% or more and had available staircase and CX3CR1 staining data. Pearson's correlation coefficient was used to determine statistical significance.

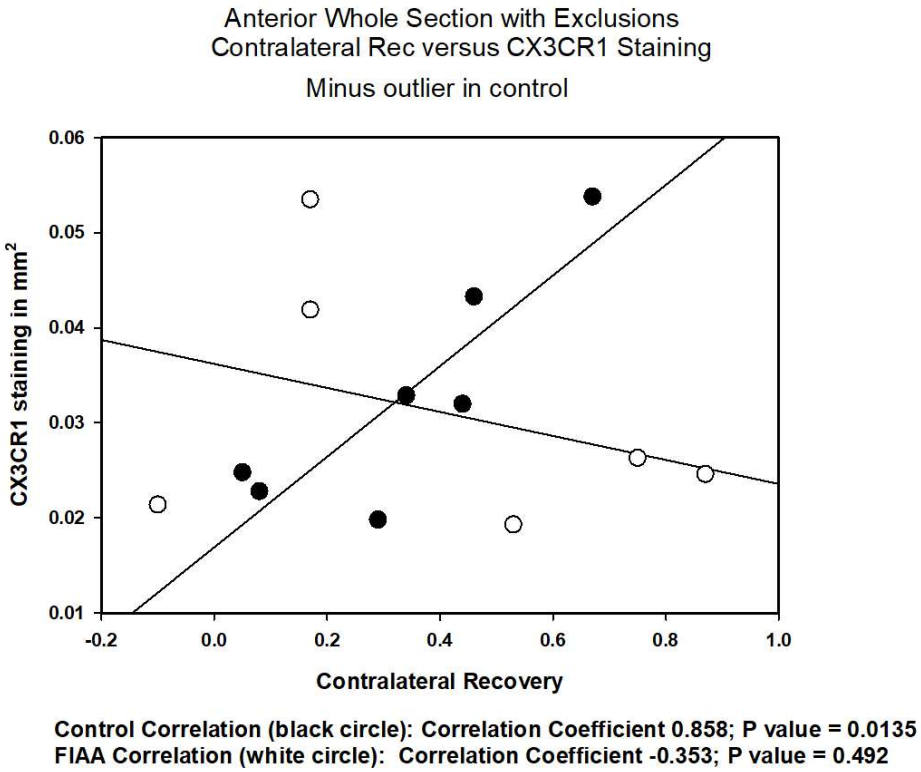

Figure 14: With removal of one outlier, control, but not treated animal recovery is well correlated with microglia in the anterior ventricle. The X-axis shows functional recovery in the forelimb contralateral to injury, while the Y-axis is CX3CR1 staining area in mm^2. Each filled circle represents one control animal (n=7) while each empty circle is a FIAA-treated animal (n=6). Pearson's correlation coefficient was used to determine statistical significance.

Middle ventricular sections were also correlated with functional recovery in the contralateral limb. We found a weak negative correlation for the FIAA-treated animals ($R=-0.409$), though it was not statistically significant ($p=0.421$). Control animals also displayed negative correlation between CX3CR1 and contralateral recovery, though it was weak ($R=-0.259$) and not statistically significant ($p=0.575$). This suggests that there is no relationship between CX3CR1 staining area in middle ventricular sections and functional recovery. However, one control animal with twice the functional recovery of any other control animal was determined to be an obvious outlier in the data set. Therefore, the correlation analysis was performed again with the exclusion of this data point. In the new correlation, control animals displayed a strong positive correlation ($R=0.802$) with very near statistical significance ($p=0.549$). This suggests that there may be a relationship between increasing CX3CR1 in middle ventricle sections and contralateral recovery that is only observed in control animals.

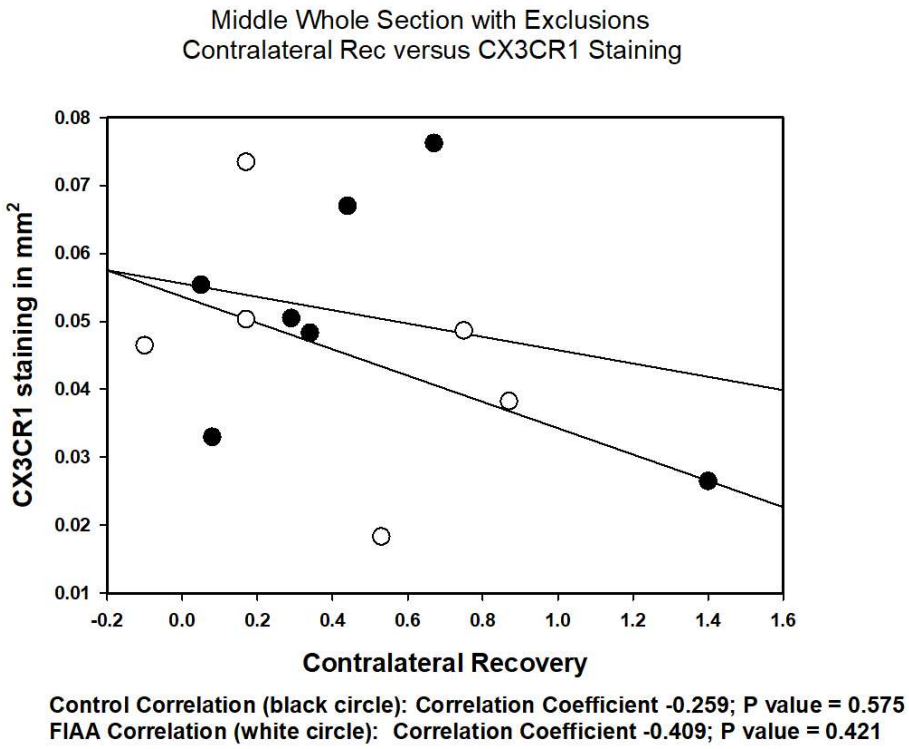

Figure 15: Middle ventricular CX3CR1 staining showed no significant correlation with contralateral recovery in controls or FIAA-treated animals. The X-axis denotes the degree of recovery in the contralateral limb while the Y-axis shows CX3CR1 staining area (in mm^2) in middle ventricular sections. Filled circles represent animals in the control group (n=7) while empty circles represent those treated with FIAA (n=6).

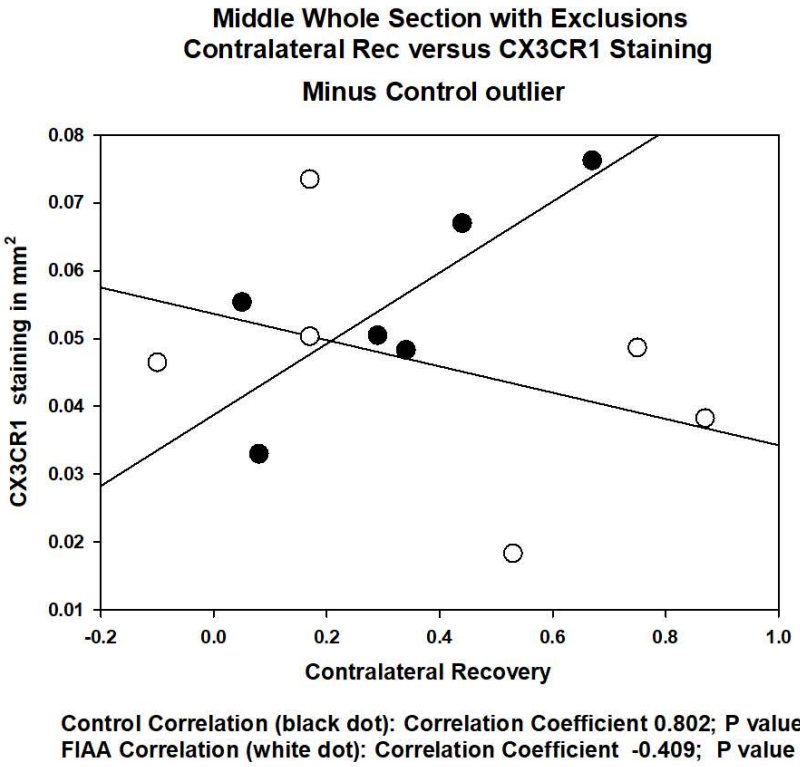

Figure 16: With the removal of an outlier, control animals now show strong positive correlation between CX3CR1 staining in middle ventricular sections and contralateral recovery. The X-axis denotes the degree of recovery in the contralateral limb while the Y-axis shows CX3CR1 staining area (in mm^2) in middle ventricular sections. Filled circles represent animals in the control group (n=6) while empty circles represent those treated with FIAA (n=6). An outlier has been removed from the control group for this correlation.

Finally, we assessed correlations between CX3CR1 staining area in posterior ventricular sections and contralateral limb recovery. For control animals, a moderate negative correlation was found (R=-0.418), though it was not statistically significant (p=0.350). FIAA-treated animals also showed a negative correlation, but it was very

weak and statistically insignificant (R=-0.0757; p=0.904). This data suggests that in posterior ventricles there is no association between the amount of CX3CR1 and the ability to recover from the injury. Because several outliers were identified in the linear regressions, they were excluded from the dataset and the correlation was repeated. Here, we again found a moderate negative correlation in controls with no statistical significance (R=-0.540; p=0.347). However, FIAA-treated animals now showed a strong negative correlation between CX3CR1 and functional recovery with statistical significance (R=-0.969; p=0.0305). These correlations suggest that posterior ventricle CX3CR1 is associated with a decrease in functional recovery with FIAA treatment but not in controls.

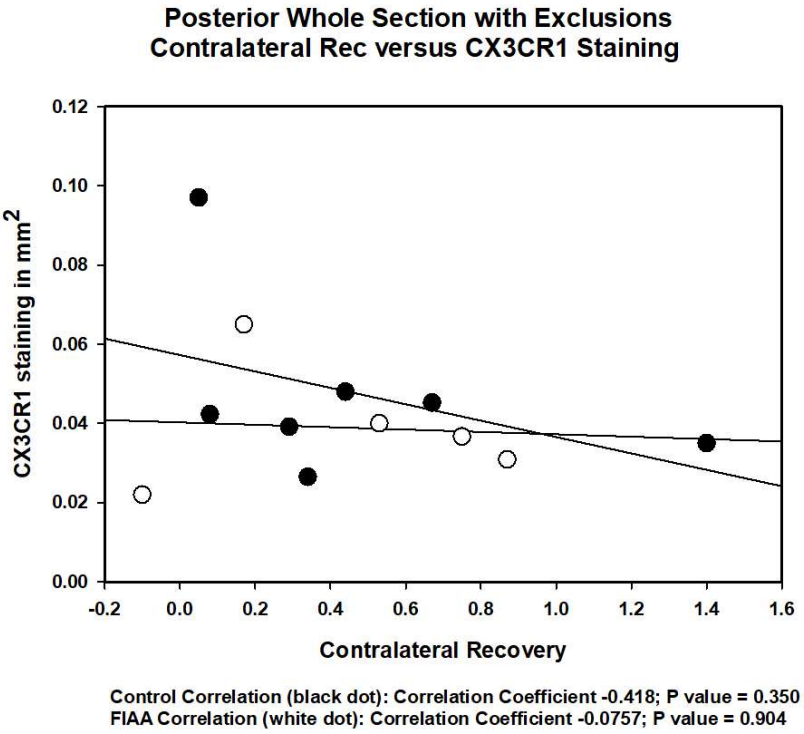

Figure 17: Posterior ventricular CX3CR1 is not associated with functional recovery in controls or FIAA-treated animals. The X-axis denotes the degree of recovery in the

contralateral limb while the Y-axis shows CX3CR1 staining area (in mm^2) in posterior ventricular sections. Filled circles represent animals in the control group (n=7) while empty circles represent those treated with FIAA (n=5).

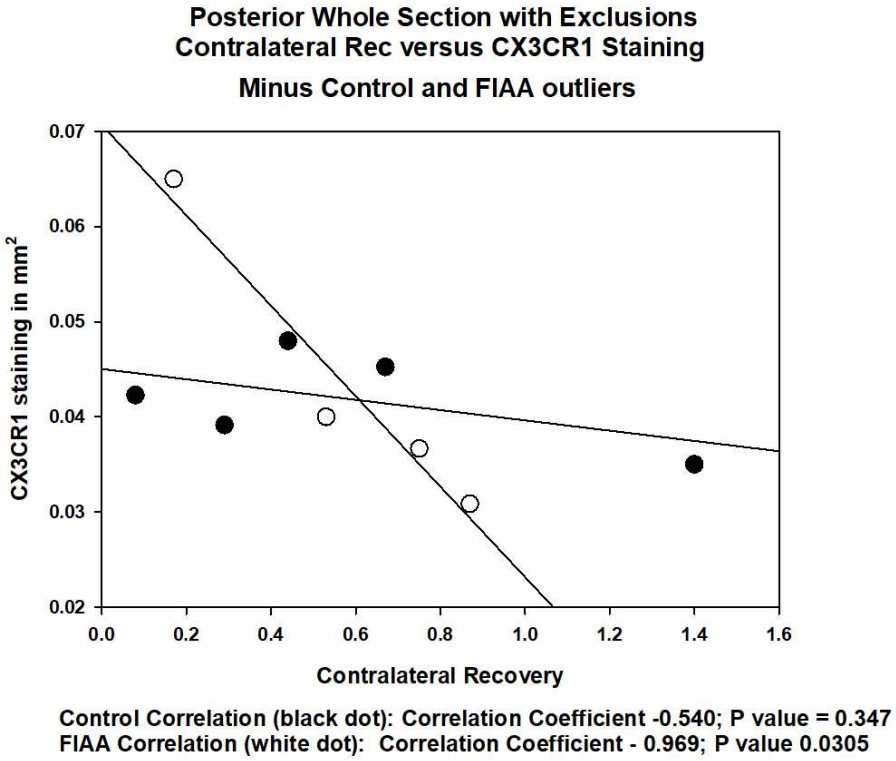

Figure 18: With the removal of outliers, FIAA animals with little posterior ventricular CX3CR1 showed greater ability to recover from the injury with the contralateral limb. The X-axis denotes the degree of recovery in the contralateral limb while the Y-axis shows CX3CR1 staining area (in mm^2) in middle ventricular sections. Filled circles represent animals in the control group (n=5) while empty circles represent those treated with FIAA (n=4). An outlier has been removed from the control group and from the FIAA treatment group for this correlation.

Because there were distinct differences in CX3CR1 staining area among anterior, middle, and posterior regions of the ventricular dorsal border, we sought to identify any correlations with functional recovery. Each region of the dorsal ventricle was plotted with functional recovery in individual animals on a linear regression. In the anterior ventricles, we identified no correlation between recovery and staining area in the corpus callosum for control animals. FIAA-treated animals showed a moderate negative correlation that was also not statistically significant ($R= -0.695$; $p=0.125$). Upon the removal of several outliers, we now observed a statistically significant and strongly positive correlation for control animals, while animals in the treatment group displayed a strongly negative correlation which was also statistically significant. This data points to an opposing relationship between contralateral recovery and dorsal anterior ventricular CX3CR1 in control versus FIAA- treated animals.

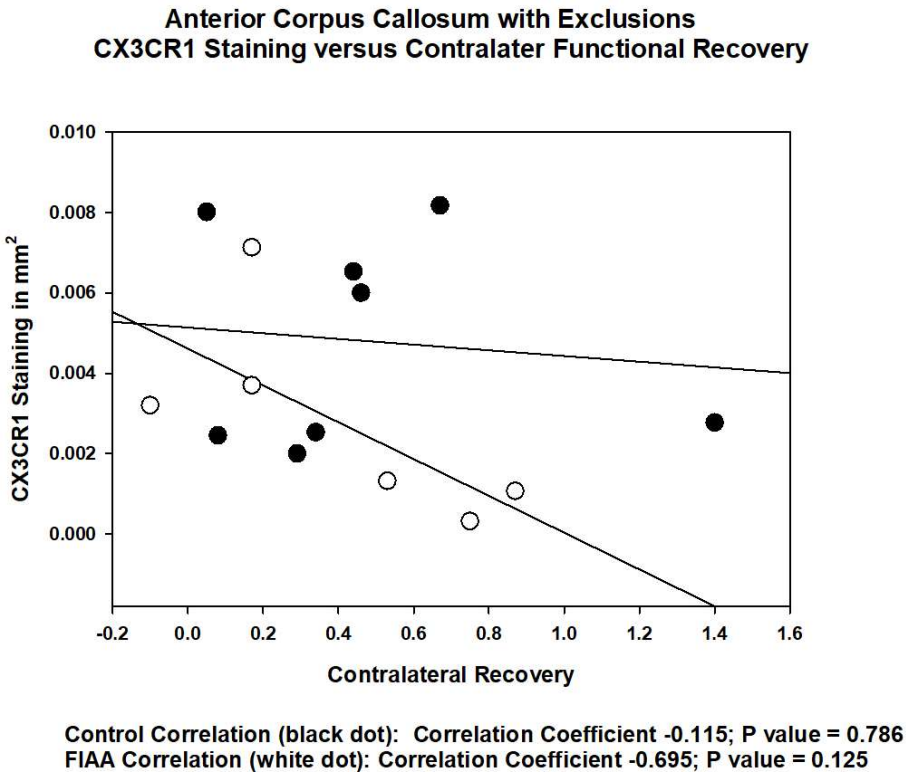

Figure 19: FIAA-treated animals with less CX3CR1 staining area in the anterior dorsal border of the ventricles showed improved functional recovery, while controls saw no significant trend. The X-axis shows functional recovery in the contralateral limb while the Y-axis shows CX3CR1 staining area (mm^2) in the dorsal border of anterior ventricular sections. Filled circles represent control animals (n=8) while hollow circles represent FIAA-treated animals (n=6).

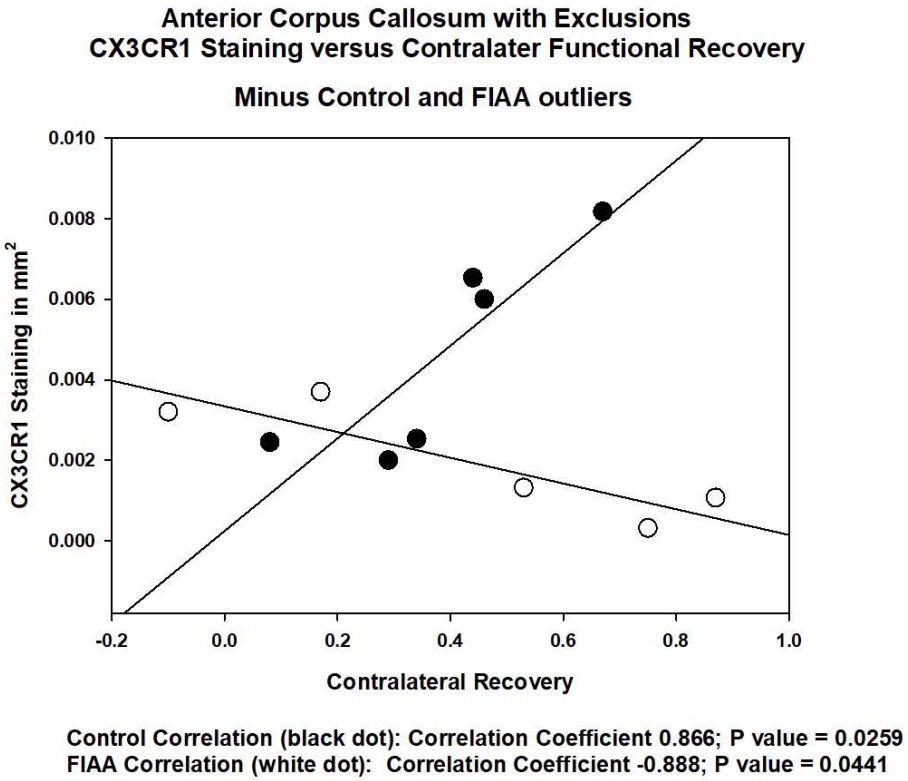

Figure 20: With the exclusion of outliers, FIAA-treated animals with less CX3CR1 staining area in the middle dorsal border of the ventricles showed improved functional recovery in the contralateral limb, while controls displayed the opposite trend. The X-axis shows functional recovery in the contralateral limb while the Y-axis shows CX3CR1 staining area (mm^2) in the dorsal border of anterior ventricular sections. Filled circles represent control animals (n=6) while hollow circles represent FIAA-treated animals (n=5).

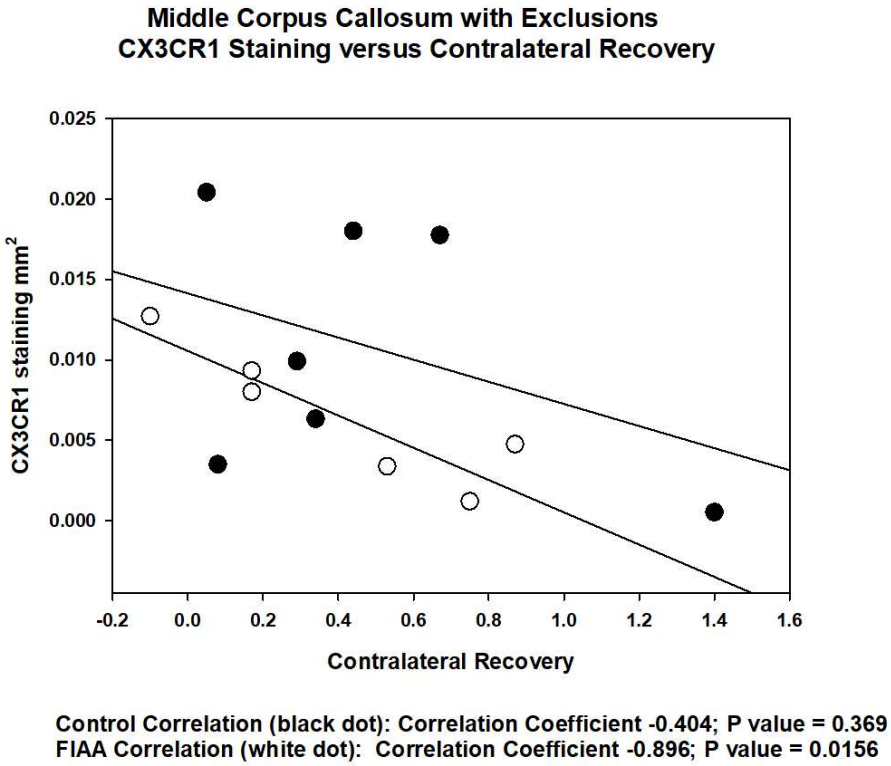

Figure 21: FIAA-treated animals with less CX3CR1 staining area in the middle dorsal border of the ventricles showed improved functional recovery in the contralateral limb. The X-axis shows functional recovery in the contralateral limb while the Y-axis shows CX3CR1 staining area (mm^2) in the dorsal border of middle ventricular sections. Filled circles represent control animals (n=7) while hollow circles represent FIAA-treated animals (n=6).

We identified a strong negative correlation in middle ventricular sections of FIAA-treated animals (R= -0.896; p=0.0156), while control animals saw a moderate negative correlation that was not statistically significant. This suggests a relationship between total microglia and functional recovery that is exclusive to treated animals. Upon the removal of control group outliers, there is now a strong positive correlation (R=0.865)

that is near statistical significance (p=0.0582). This data indicates that there exists a relationship between CX3CR1 staining area and contralateral recovery in the FIAA-treatment group that may be inverse compared with controls.

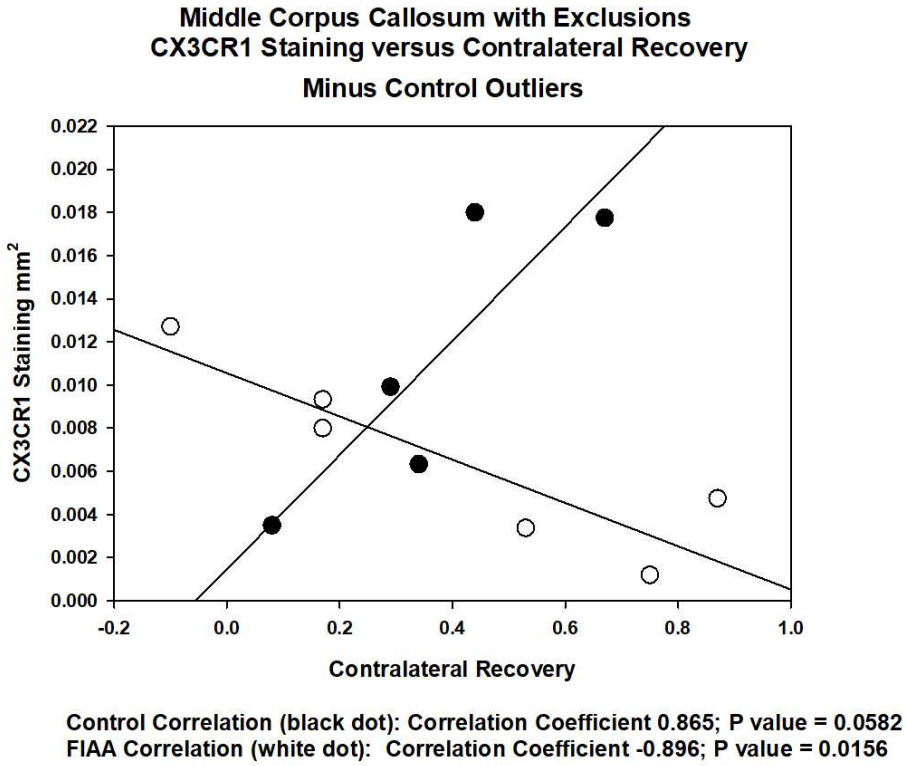

Figure 22: Upon the exclusion of outliers in the control group, control animals now show a near-significant strongly positive correlation between CX3CR1 staining area in the dorsal border of middle ventricular sections and contralateral functional recovery. The X-axis shows functional recovery in the contralateral limb while the Y-axis shows CX3CR1 staining area (mm^2) in the dorsal border of middle ventricular sections. Filled circles represent control animals (n=5) while hollow circles represent FIAA-treated animals (n=6). Two outliers have been removed from the control group for this analysis.

Finally, we compared contralateral recovery with staining area in the dorsal border (corpus callosum adjacent) of posterior ventricular sections for control and FIAA-treated animals. We found a strongly negative correlation in control (R= -0.856) and FIAA-treated animals (R= -0.798) which was only statistically significant in control animals (p=0.0141). One animal in the FIAA group was identified as an outlier, so the regression was plotted again with the removal of this data point. Here, we found a strongly negative correlation in the FIAA treatment group that was statistically significant (R= -0.985; p=0.0149). This data suggests an inverse relationship between CX3CR1 in the posterior ventricles and functional recovery, regardless of treatment.

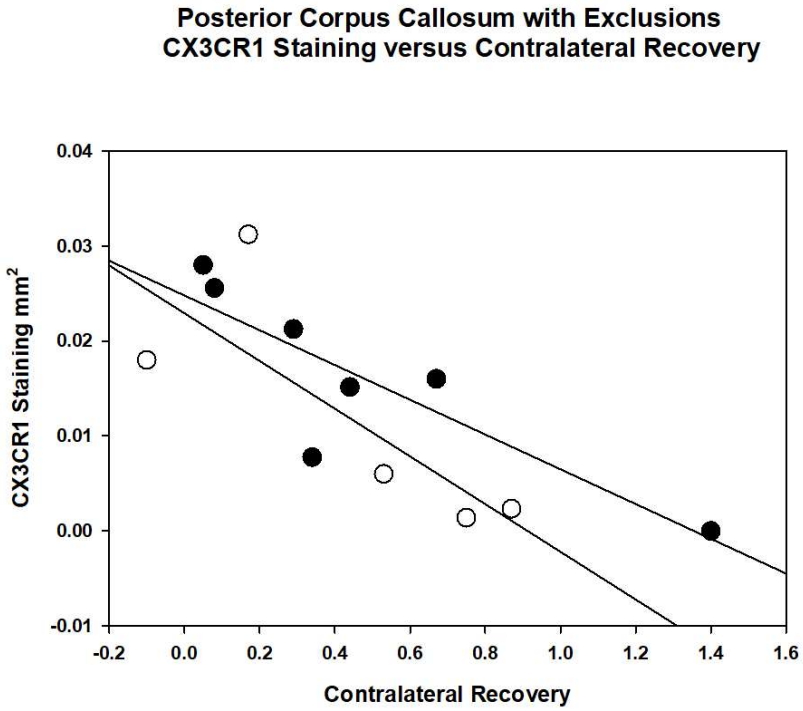

Figure 23: Contralateral functional recovery is strongly negatively correlated with CX3CR1 staining area in the dorsal border of posterior ventricular sections of control animals. The X-axis shows functional recovery in the contralateral limb while the Y-axis shows CX3CR1 staining area (mm^2) in the dorsal border of posterior ventricular sections. Filled circles represent control animals (n=7) while hollow circles represent FIAA-treated animals (n=5).

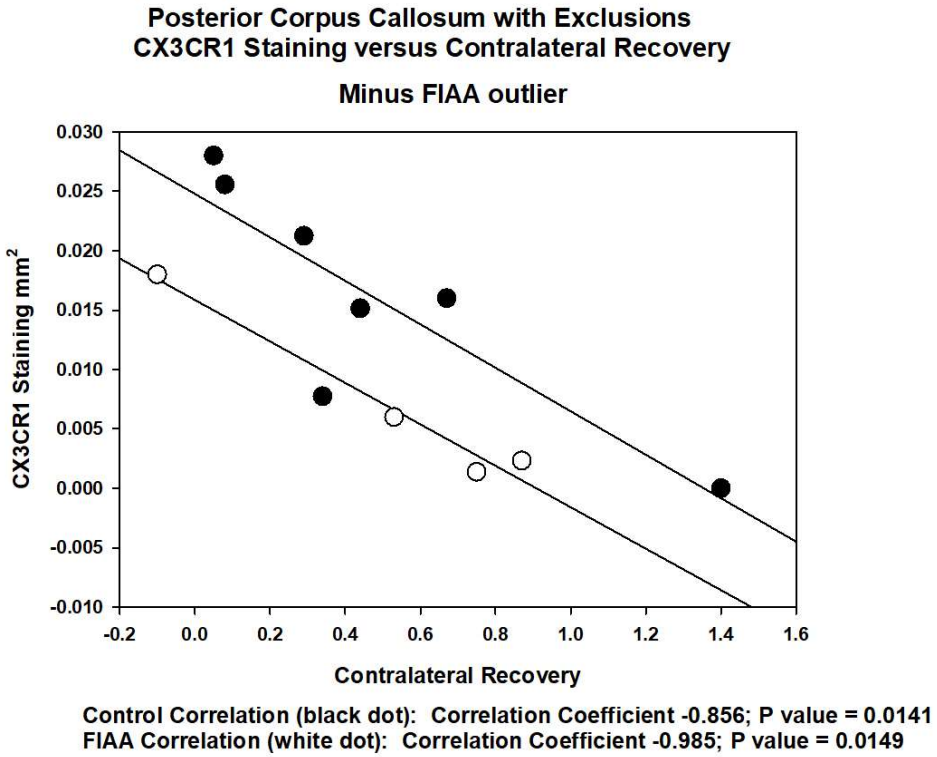

Figure 24: With the removal of an outlier in the treatment group, contralateral functional recovery is negatively correlated with CX3CR1 staining area in the dorsal border of posterior ventricular sections of control and FIAA-treated animals. The X-axis shows functional recovery in the contralateral limb while the Y-axis shows CX3CR1 staining area (mm^2) in the dorsal border of posterior ventricular sections. Filled circles represent

control animals (n=7) while hollow circles represent FIAA-treated animals (n=4). An outlier has been removed from the treatment group for this correlation.

We found that CX3CR1 staining area is correlated with contralateral functional recovery in each examined area of the ventricles, though the specific correlations vary widely by region and by treatment. Anterior and near the corpus callosum, CX3CR1 is associated with an increase in functional recovery in control animals, but a decrease in FIAA-treated animals. Activated microglia in the corpus callosum have been shown to cause substantial damage to the white matter tract (Zhang et al., 2021). Therefore, the negative correlation of CX3CR1 area and functional recovery suggests the diminished area is not due to a larger proportion of activated microglia as this would be deleterious to recovery in the ipsilateral limb, though conclusions about microglial activation cannot be made from this CX3CR1 data alone. The opposing trends in controls may be due to several distinct reasons. Control animals see a positive correlation in the anterior of the ventricles possibly because of the activation status of microglia present – more microglia in the branched (inactivated) state would yield a better recovery by lowering inflammation and directly cause higher CX3CR1 staining area. The positive correlation is unlikely to be due to a larger number of microglia present, as microglia count reduction has been deemed beneficial to recovery in several injury models (Henry et al., 2020; Poulen et al., 2021). Conversely, recovery in FIAA-treated animals may be more significantly determined by the phenotype of microglia that aid in recovery. As Iba-1^{-}/CX3CR1^{+} microglia often have less surface area than most microglial subtypes (Ribiero-

Xavier et al., 2015), it is possible the association with less CX3CR1 area is due to the relative increase in this subtype within the pool of microglia.

As we moved more posterior with the dorsal border ventricle sections, the positive correlation of CX3CR1 area and recovery diminishes into only nearly statistically significant in middle sections before reversing to a significant negative correlation in posterior sections. A similar trend was observed in control sections of whole ventricular sections, though the posterior saw no correlation. A decrease in CX3CR1 area may be due to a beneficial microglia subtype gradient observed anterior to posterior in which Iba-1^{-}/CX3CR1^{+} microglia are more concentrated in the posterior ventricles, and animals which had alternative gradients recovered less. This association may implicate Iba-1^{-}/CX3CR1^{+} microglia in a regional specificity for injury recovery. A summary of the correlations data is shown on the following pages in Table 4 and Table 5.

Table 4

Anterior			
	Correlation Coefficient	Strength/Direction	P value
Control	0.477	Moderate positive	0.232
Control minus outlier	0.858	Strong positive	0.0135
FIAA	-0.353	Weak negative	0.492

Middle			
	Correlation Coefficient	Strength/Direction	P value
Control	-0.259	Weak negative	0.575
Control minus outlier	0.802	Strong positive	0.0549
FIAA	-0.409	Moderate negative	0.421

Posterior			
	Correlation Coefficient	Strength/Direction	P value
Control	-0.418	Moderate negative	0.350
Control minus outlier	-0.540	Moderate negative	0.347
FIAA	-0.0757	Weak negative	0.904
FIAA minus outlier	-0.969	Strong negative	0.0305

Table 5

Anterior CC			
	Correlation Coefficient	Strength/Direction	P value
Control	-0.115	Weak negative	0.786
Control minus outlier	0.866	Strong positive	0.0259
FIAA	-0.695	Moderate negative	0.125
FIAA minus outlier	-0.888	Strong negative	0.0441

Middle CC			
	Correlation Coefficient	Strength/Direction	P value
Control	-0.404	Moderate negative	0.369
Control minus outlier	0.865	Strong positive	0.0582
FIAA	-0.896	Strong negative	0.0156

Posterior CC			
	Correlation Coefficient	Strength/Direction	P value
Control	-0.856	Strong negative	0.0141
FIAA	-0.798	Strong negative	0.105
FIAA minus outlier	-0.985	Strong negative	0.0149

IV. DISCUSSION

Montoya Staircase

The Montoya staircase test is a unilateral measure of forelimb motor capabilities in rats. Here, we have applied the test to 10-11-month-old female Sprague-Dawley rats to assess functional recovery after treatment of a demyelinating lesion. We established a baseline function in the animals before inducing the injury, then treated the animals with FIAA and assessed recovery versus controls at four additional time points post-surgery.

Control and treated animals displayed similar initial deficits in both the contralateral and ipsilateral limbs. Contralateral deficits were much larger than those of the ipsilateral, with a function decrease of nearly 40% versus ~10%, respectively. The target site for the injury was the right corpus callosum, so we predicted both an ipsilateral and contralateral deficit as seen in prior corpus callosum injuries (Price and Fowler, 1981). Interestingly, we observed a much larger contralateral deficit compared with that of the ipsilateral limb. This effect is most likely due to an injection discrepancy not seen in prior experiments. One possibility is the injecting syringe was not sufficiently deep into the cranium, causing injury superior to the intended target. This would largely spare the corpus callosum and instead damage the forelimb motor cortex, leading to a large contralateral deficit as we observed here.

Because the treatment regimen is started six days after the induction of the injury, Montoya staircase scoring on post-surgery day 15 is the earliest day the effect of the drugs can be observed. Ipsilateral limbs of FIAA-treated rats showed a noticeable decrease in function on this day compared to post-surgery day 3 and controls (see Figure 9). This pattern is most likely due to a drug effect as it only occurs in treated animals and not controls. It is possible that the phenotype shift in microglia is occurring during the period between the first day of drug treatment and post-surgery day 15, and future experiments including data on microglial activation states may be better suited to evaluate this possibility. Inflammatory cytokines such as TNF-α and IL-6 would thus be reduced and anti-inflammatory cytokines such as IL-4 and IL-10 would be increased. As inflammatory cytokines are known to have protective effects immediately after injury (Rossi et al., 2021), this shift from M1 to M2 microglia may decrease limb function by eliminating early helpful inflammation.

Another possibility may be that microglia are activated before their phenotypes shift from inflammatory to anti-inflammatory. This would cause an increase in inflammatory cytokines that is harmful to newborn OPCs, leading to reduced early remyelination and the increased deficit observed in the ipsilateral limb. Indeed, a similar effect has been observed in hippocampal neurogenesis. Inflammatory cytokines IL-1β and IL-6 have both been shown to have detrimental effects on neurogenesis of hippocampal cells (Goshen et al., 2008; Monje et al., 2003). Specific interactions of inflammatory and anti-inflammatory cytokines with neurogenesis must be further investigated to develop methods for harnessing inflammation to enhance neurogenesis.

Interestingly, this effect can only be observed in the ipsilateral limb and not in the contralateral limb. A possible explanation for this difference is the magnitude of the initial deficit. As contralateral deficits were much larger than ipsilateral, recovery can more easily be observed and the harmful effects of the M1-M2 phenotype shift may be masked. In the ipsilateral limbs, deficits were sufficiently small that the effect is apparent, and recovery was too small to mask the effect. In the future, larger ipsilateral deficits and smaller contralateral deficits should be achieved to study this effect. We would expect the effect to be observable in the contralateral limb if the deficit is small enough, and the effect to be masked in the ipsilateral limb if the deficit is sufficient.

Microglia

Serving as the primary mediators of inflammation, microglia are important for maintaining homeostasis in the CNS. It has recently been accepted that microglia are a diverse cell type with a variety of functions and subtypes (Stratoulias et al., 2019). Here, we found that microglia are localized in the posterior SVZ region in greater amounts than in the anterior region. Distribution of microglia positive for CX3CR1 does not appear to be significantly affected by our drug combination of fluoxetine, ibuprofen, and ascorbic acid across the whole ventricle. Because the injection of lysolecithin was localized in the anterior region of the ventricle, it is possible that the reduction of microglia in this region is due to the lysolecithin. It has been shown previously that lysolecithin exposure to microglia results in a reduction of ramifications and an ameboid morphology (Schilling et al., 2004), although this was examined over just a 60-minute period *in vitro* while our

study involves *in vivo* exposure at 48 days after injection. Additionally, it has not been shown whether lysolecithin itself induces cell death in microglia, yet the function may be temporarily affected by de-ramification. Due to the extended delay of microglia examination after lysolecithin exposure and the environmental distinction it is not likely that the microglia gradient observed here is a result of lysolecithin itself, but comparison to uninjured and saline-injected animals must be performed to determine if the injury is inducing the microglia gradient observed here, or if this is an inherent property of the ventricles.

Demyelination from lysolecithin injection is often localized to the corpus callosum. This led us to analyze CX3CR1 positive microglia in this region specifically. We found a similar regional correlation here as with the whole ventricle. There was no effect of FIAA treatment on the microglia distribution near the corpus callosum. Treatment with FIAA combination therefore does not affect $CX3CR1^{+}$ microglia proliferation and/or migration in the SVZ. However, the activation or phenotype of these microglia cannot be determined from these results alone. Iba-1 and CD68 immunoreactivity compared with these results would be useful in determining if the drug combination changes the phenotype or reactivity of these microglia. Assays for cytokines such as IL-4 and IL-10 in the tissue would allow measurements of the microglial activity as well and possibly show an effect on these microglia that cannot be determined from CX3CR1 staining alone. Activation state of microglia would be important additional information since IL-4 and IL-10 are necessary for migration of neuroblasts into the olfactory bulb (Ribiero-Xavier et al., 2015) and fluoxetine is thought to be switching

microglia into a neuroprotective phenotype. It may be that the combination treatment of FIAA does not affect the migration or proliferation of microglia but does alter their activation state and/or phenotype.

After completion of the microglia staining described here, we were informed that the reliability of the antibody used for CX3CR1 is now in question. The supplier has withdrawn availability of the antibody due to the failure to pass a genetic knockout verification for CX3CR1 labelling in a THP-1 cell lysate, although no negative control was used. Nevertheless, caution must be given when interpretating the staining results presented here. However, translation of the antibody from THP-1 cells to microglia may be limited, as the two immune cells are vastly different, serving different functions and existing naturally far removed from one another. Additionally, the antibody is likely labelling microglia as the staining pattern observed is representative of that seen with other antibodies used on the tissue collected from these animals: In Figure 5 the characteristic distribution of microglia can be seen using two other microglial markers Iba1 and CD11c, and the darkened staining around the subventricular zone is like that of CX3CR1 in Figure 4. The concentration of CX3CR1 expression around the lateral ventricles is consistent with reports examining RNAseq data in mice such as that detailed in Figure 25.

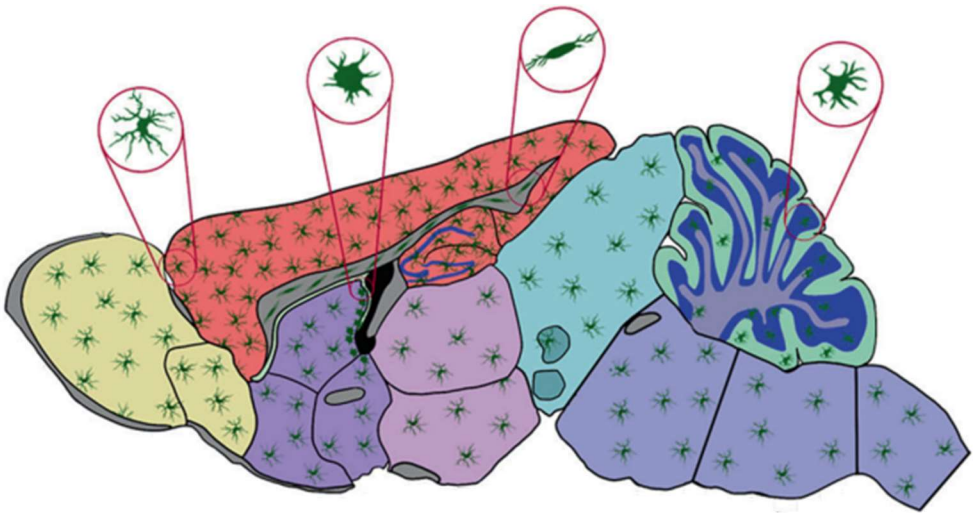

Figure 25: Microglia assume a wide variety of morphologies and distributions in different mouse brain regions. The representative microglia shapes are shown in circle insets. Microglia are concentrated at the border of the lateral ventricles and conform to an ameboid shape while corpus callosum microglia are shown as rod-shaped with relatively low amounts. Figure modified from Tan et al., 2020.

Correlations

Interestingly, in each area of the ventricle we examined, FIAA treatment yielded a correlation that was more of a linear inverse relationship than the control counterparts. The areas in which a positive relationship was observed in the controls were made negative with FIAA treatment, and negative correlations were stronger with treatment than without. There are three possibilities for this pattern: 1) treatment favors recovery in animals which have less branched microglia; 2) treatment favors recovery in animals with

less microglia cell counts; 3) treatment favors recovery in animals that have microglia with less CX3CR1 expression.

The first possibility can be explained by the increase in branching microglia experience as aging occurs, meaning that animals which are less affected by signs of aging are better suited for the treatment. As microglia branching is reduced with activation, it may be true that activated microglia are beneficial for injury recovery. This idea is supported by findings showing that activated microglia are protective against cryogenic lesion injury in mice (Chen et al., 2014), though the recovery from the injury was not evaluated over time. A decrease in branching may also be from a subtype difference. As Iba-1^{-}/CX3CR1^{+} microglia branch less than others (Ribiero-Xavier et al., 2015), differences in their distribution would imply a difference in surface area that we observe by CX3CR1 staining area. The second of these possibilities, if true, would suggest that microglia overall can be harmful to injury recovery when present in high populations, and the treatment exacerbates this issue.

As for the third possibility, it has been observed that CX3CR1 and its ligand can induce an anti-inflammatory phenotype in microglia (Lauro et al., 2019), thus a decrease in the expression of the receptor would likely be harmful to recovery as microglia would exist in a more inflammatory role. However, certain effects of the receptor may be harmful to recovery as CX3CR1 has been implicated in neuron loss in a mouse model of Alzheimer's Disease (Furhmann et al., 2010). Genetic knockout of CX3CR1 has also been shown to be beneficial to injury recovery and inflammation in a mouse model of ischemic stroke (Denes 2008), possibly through the reduction of IL-1β and TNF-α.

Increased microglial CX3CR1 expression levels also increase their migration (Cao et al., 2019), suggesting that microglia with lower expression may have a diminished ability to accumulate near the injury site without an increase in proliferation. The treatment may be favoring recovery in animals with lower levels of highly mobile (high CX3CR1 expressing) microglia.

When considering these correlations, we must also account for the proximity to the location of the injury. Our injection, at the most posterior point, was near bregma, corresponding to sections in the middle of the lateral ventricles. As the injury was focused on the anterior and middle sections, the posterior was expected to be largely spared from damage by the lysolecithin. In a post-mortem analysis of MS patients' brains, it was shown that microglia are highly proliferative in active lesions and in normal appearing white matter when compared to controls (Nowacki et al., 2019). Additionally, microglial surface protein expression changes drastically in response to injury and these changes are variable between microglial subpopulations (Gottlieb et al., 2022). Thus, MS lesions, like the injury we have modeled here, may have some effect on the distribution of microglia in the ventricles and affect microglial subtypes differentially. To parse these effects on microglia, future experiments with similar methods may benefit from implementing an animal group with treatment and no injury or sham injury. Future experiments would benefit from using multiple microglial markers to distinguish subtypes and how their distribution is affected by the drugs.

Conclusion

Multiple sclerosis patients face severe detriment to quality of life (Gustavsen et al., 2021), and this is especially true for the older population. As MS prevalence grows with the aging population, the need for effective treatments grows as well. Here, we have implemented an *in vivo* model of MS to deduce the effects of fluoxetine, ibuprofen, and ascorbic acid on functional recovery and microglia in the lateral ventricles. Microglia display region-dependent distributions within the ventricles which are largely unchanged by treatment. Recovery and CX3CR1 correlations change significantly with treatment, but more work is necessary to fully understand the relationships between functional recovery and CX3CR1 in MS.

V. APPENDIX

Table 6: Reagents

Reagent	**Source**	**Identifier**	**Use**
CX3CR1 antibody	AbCam	ID: ab217191	Microglia labelling
VECTASTAIN elite ABC kit (Anti-rabbit)	Vector Labs	Lot: PK-6101	Antibody staining
BLOXALL Blocking Solution	Vector Labs	SKU: SP-6000-100	Antibody blocking
DPX Mountant	Sigma Aldrich	Lot: 06522	Mountant
L-α-lysophosphatidylcholine (Lysolecithin; 1%)	Sigma Aldrich	Lot: SLCH3510	Demyelination
Fluoxetine (5mg/kg)	CVS, Generic	N/A	Treatment
Ibuprofen (20mg/kg)	Generic	Lot: B61010	Treatment
Ascorbic Acid (50mg/kg)	Fluka	Lot: 95209	Treatment
Sugar Cookie Dough	Pillsbury	N/A	Treatment Vehicle

VI. REFERENCES

Allred RP, Cappellini CH, Jones TA. The “good” limb makes the “bad” limb worse: Experience-dependent interhemispheric disruption of functional outcome after cortical infarcts in rats. Behav Neurosci. 2010. (124):124-132. doi: 10.1037/a0018457

Andersson M, Alvarez-Cermeño J, Bernardi G, Cogato I, Fredman P, Frederiksen J, Frederikson S, Gallo P, Grimaldi LM, Gronning M, Keir G, Lamers K, Link H, Magalhaes A, Massaro AR, Ohman S, Reiber H, Ronnback L, Schluep M, Schuller E, Sindic CJM, Thompson EJ, Trojano M, Wurster U. Cerebrospinal fluid in the diagnosis of multiple sclerosis: a consensus report. Journal of Neurology, Neurosurgery, and Psychiatry. 1994. (57):897-902.

Bachstetter AD, Morganti JM, Jernberg J, Schlunk A, Mitchell SH, Brewster KW, Hudson CE, Cole MJ, Harrison JK, Bickford PC, Gemma C. Fractalkine and CX3CR1 regulate hippocampal neurogenesis in adult and aged rats. Neurobiol Aging. 2011. (32):2030-2044. doi:1016/j.neurobiolaging.2009.11.022

Benmamar-Badel A, Owens T, Wlodarczyk A. Protective microglial subset in development, aging, and disease: lessons from transcriptomic studies. Front Immunol. 2020. (11):430. doi: 10.3389/fimmu.2020.00430

Cao R, Li S, Yin J, Guo L, Shi J. Sirtuin 3 promotes microglia migration by upregulating CX3CR1. Cell Adhesion and Migration. 2019. (13):228-234. doi: 10.1080/19336918.2019.1629224

Cardona AE, Pioro EP, Sasse ME, Kostenko V, Cardona SM, Dijkstra IM, Huang D, Kidd G, Dombrowski S, Dutta R, Lee JC, Cook DN, Jung S, Lira SA, Littman DR, Ransohoff RM. Control of microglial neurotoxicity by the fractalkine receptor. Nature Neuroscience. 2006. (9):917-924. doi:10.1038/nn1715

Cencioni MT, Ali R, Nicholas R, Muraro PA. Defective CD19+CD24hiCD38hi transitional B-cell function in patients with relapsing-remitting MS. Multiple Sclerosis Journal. 2021. (27):1187-1197. doi: 10.1177/1352458

Chataway J, De Angelis F, Connick P, Parker RA, Plantone D, Doshi A, John N, Stutters J, MacManus D, Carrasco FP, Barkhof F, Ourselin S, Braisher M, Ross M, Cranswick G, Pavitt SH, Giovannoni G, Wheeler-Kingshott CAG, Hawkins C, Sharrack B, Bastow R, Weir CJ, Stallard N, Chandran S. Efficacy of three neuroprotective drugs in secondary progressive multiple sclerosis (MS-SMART): a phase 2b, multiarm, double-blind, randomized placebo-controlled trial. Lancet. 2020. (19):214-225. doi: 10.1016/S1474-4422(19)30485-5

Chataway J, Schuerer N, Alsanousi A, Chan D, MacManus D, Hunter K, Anderson V, Bangham CRM, Clegg S, Nielsen C, Fox NC, Wilkie D, Nicholas JM, Calder VL, Greenwood, Frost C, Nicholas R. Effect of high-dose simvastatin on brain atrophy and disability in secondary progressive multiple sclerosis (MS-STAT): a

randomized, placebo-controlled, phase 2 trial. Lancet. 2014. (383):2213-2221. doi: 10.1016/S0140-6736(13)62242-4

Chen z, Jalabi W, Hu W, park JW, Gale JT, Kidd GJ, Bernatowicz R, Gossman ZC, Chen JT, Dutta R, Trapp BD. Microglial displacement of inhibitory synapses provided neuroprotection in the adult brain. Nature Communications. 2014. (5):4486. doi: 10.1038/ncomms5486

Cherry JD, Olschowka JA, O'Banion MK. Neuroinflammation and M2 microglia: the good, the bad, and the inflamed. J Neuroinflammation. 2014. (11):98. doi: 10.1186/1742-2094-11-98

Cignarella F, Filipello F, Bollman B, Cantoni C, Locca A, Mikesell R, Manis M, Ibrahim A, Deng L, Benitez BA, Cruchaga C, Licastro D, Mihindukulasuriya K, Harari, Buckland M, Holtzman DM, Rosenthal A, Schwabe T, Tassi I, Piccio L. TREM2 activation on microglia promotes myelin debris clearance and remyelination in a model of multiple sclerosis. Acta Neuropathologica. 2020. (140):512-534. doi: 10.1007/s00401-020-02193-z

Corbett A, McGowin A, Sieber S, Flannery T, Sibbitt B. A method for reliable voluntary oral administration of a fixed dosage (mg/kg) of chronic daily medication to rats. Lab Anim. 2012. (46):318-324. doi: 10.1258/la.2012.012018

Corbett AM, Sieber S, Wyatt N, Lizzi J, Flannery T, Sibbit B, Sanghvi S. Increasing neurogenesis with fluoxetine, simvastatin, and ascorbic acid leads to functional

recovery in ischemic stroke. Recent Patents on Drug Delivery & Formulation. 2015. (9):000. doi: 10.2174/1872211309666150122102846

Deisenhammer F, Zetterberg H, Fitzner B, Zettl UK. The cerebrospinal fluid in multiple sclerosis. Front Immunol. 2019. (10):726. doi: 10.3389/fimmu.2019.00726

Denes A, Ferenczi S, Halasz J, Kornyei Z, Kovacs KJ. Role of CX3CR1 (fractalkine receptor) in brain damage and inflammation induced by focal cerebral ischemia in mouse. Journal of Cerebral Blood Flow and Metabolism. 2008. (28):1707-1721. doi: 10.1038/jcbfm.2008.64

Elsisi NS, Darling-Reed S, Lee EY, Oriaku ET, Soliman KF. Ibuprofen and apigenin induce apoptosis and cell cycle arrest in activated microglia. Neuroscience Letters. 2005. (375):91-96. doi: 10.1016/j.neulet.2004.10.087

Frank MG, Barrientos RM, Biedenkapp JC, Rudy JW, Watkins LR, Maier SF. mRNA up-regulation of MHCII and pivotal pro-inflammatory genes in normal aging. Neurobiol Aging. 2006. (27):717-722. doi: 10.1016/j.neurobiolaging.2005.03.013

Furhmann M, Bittner T, Jung CKE, Burgold S, Page RM, Mitteregger G, Haass C, LaFerla FM, Kretzschmar H, Herms J. Microglial CX3CR1 knockout prevents neuron loss in a mouse model of Alzheimer's disease. Nature Neurosci. 2010. (13):411-413. doi: 10.1038/nn.2511

Gholamzad M, Ebtekar M, Ardestani MS, Azimi M, Mahmodi Z, Mousavi MJ, Aslani S. A comprehensive review on the treatment approaches of multiple sclerosis:

currently and in the future. Inflammation Research. 2019. (68):25-38. doi: 10.1007/s00011-018-1185-0

Goldschmidt C, McGinley MP. Advances in the treatment of multiple sclerosis. Neurol Clin. 2021. (39):21-33. doi:10.1016/j.ncl.2020.09.002

Goshen I, Krisel T, Ben-Menachem-Zidon O, Licht T, Weidenfeld J, Ben-Hur T, Yirmiya R. Brain interleukin-1 mediates chronic stress-induced depression in mice via adrenocortical activation and hippocampal neurogenesis suppression. Molecular Psychiatry. (13):717-728. doi: 10.1038/sj.mp.400205

Gottlieb A, Toledano-Furman N, Prabhakara KS, Kumar A, Caplan HW, Bedi S, Cox Jr CS, Olson SD. Time dependent analysis of rat microglial surface markers in traumatic brain injury reveals dynamics of distinct cell subpopulations. Scientific Reports. 2022. (12):6289. doi: 10.1038/s41598-022-10419-1

Guo YE, Suo N, Cui X, Yuan Q, Xie X. Vitamin C promotes oligodendrocytes generation and remyelination. Glia. 2018. (66):1302-1316. doi: 10.1002/glia.23306

Gustavsen S, Olsson A, Sondergaard HB, Andresen ST, Sorensen PS, Sellebjerg F, Oturai A. The association of selected multiple sclerosis symptoms with disability and quality of life: a large Danish self-report survey. BMS Neurology. 2021. (21):317. doi: 10.1186/s12883-021-02344-z

Gyoneva S, Hosur R, Gosselin D, Zhang B, Ouyang Z, Cotleur AC, Peterson M, Allaire N, Challa R, Cullen P, Roberts C, Miao K, Reynolds TL, Glass CK, Burkly L,

Ransohoff RM. CX3CR1-deficient microglia exhibit a premature aging transcriptome. Life Sciences Alliance. 2019. doi:10.26508/lsa.201900453

Harrison JK, Jiang Y, Chen S, Xia Y, Maciejewski D, McNamara RK, Streit WJ, Salafranca MN, Adhikari S, Thompson DA, Botti P, Bacon KB, Feng L. Role for neuronally derived fractalkine in mediating interaction between neurons and CX3CR1-expressing microglia. Neurobiology. 1998. (95):10896-10901

Hauser SL, Cree BAC. Treatment of multiple sclerosis: A review. Am J Med. 2020. (133):1380-1390. doi: 10.1016/j.amjmed.2020.05.049

Henry RJ, Ritzel RM, Barrett JP, Doran SJ, Jiao Y, Leach JB, Szeto GL, Wu J, Stoica BA, Faden AI, Loane DJ. Microglial depletion with CSF1R inhibitor during chronic phase of experimental traumatic brain injury reduces neurodegeneration and neurological deficits. J Neurosci. 2020. (40):2960-2974. doi: 10.1523/JNEUROSCI.2402-19.2020

Huppert J, Closhen D, Croxford A, White R, Kulig P, Pietrowski E, Bechmann I, Becher B, Luhmann HJ, Waisman A, Kuhlmann CRW. Cellular mechanisms of IL-17-induced blood-brain barrier disruption. FASEB J. 2010. (24):1023-1034. doi: 10.1096/fj.09-141978

Imai T, Heishima K, Haskell C, Baba M, Nagira M, Nishimura M, Kakizaki M, Takagi S, Nomiyama H, Schall T, Yoshie O. Identification and molecular characterization of fractalkine receptor CX3CR1, which mediates both leukocyte migration and adhesion. Cell. 1997. (91):521-530.

Kamm CP, Uitdehaag BM, Polman CH. Multiple sclerosis: Current knowledge and future outlook. Eur Neurol. 2014. (72):132-141. doi: 10.1159/000360528

Klineova S, Lublin FD. Clinical course of multiple sclerosis. Cold Spring Harb Perspect Med. 2018. (8):a028928. doi: 10.1101/cshperspect.a028928

Kloth V, klein A, Loettrich D, Nikkhah G. Colour-coded pellets increase the sensitivity of the staircase test to differentiate skilled forelimb performances of control and 6-hydroxydopamine lesioned rats. Brain Research Bulletin. 2006. (70):68-80. doi: 10.1016/j.brainresbull.2006.04.006

Kunkl M, Frascolla S, Amormino C, Volpe E, Tuosto L. T helper cells: The modulators of inflammation in multiple sclerosis. Cells. 2020. (9):482. doi: 10.3390/cells9020482

Lauro C, Chece G, Monaco L, Antonangeli F, Peruzzi G, Rinaldo S, Paone A, Cutruzzola F, Limatola C. Fractalkine modulates microglia metabolism in brain ischemia. Front. Cell. Neurosci. 2019. (13):414. doi: 10.3389/fncel.2019.00414

Lee CK, Weindruch R, Prolla TA. Gene-expression profile of the ageing brain in mice. Nature Genetics. 2000. (25):294-297. doi: 10.1038/77046

Lenzi D, Conte A, Mainero C, Frasca V, Fubeli F, Totaro P, Caramia F, Inghilleri M, Pozzilli C, Pantano P. Effect of corpus callosum damage on ipsilateral motor activation in patients with multiple sclerosis: A functional and anatomical study. Hum Brain Mapp. 2007. (7):636-644. doi: 10.1002/hbm.20305

Liddelow SA, Guttenplan KA, Clarke LE, Bennett FC, Bohlen CJ, Schirmer L, Bennet ML, Munch AE, Chung WS, Peterson TC, Wilton DK, Frouin A, Napier BA, Panicker N, Kumar M, Buckwalter MS, Rowitch DH, Dawson VL, Dawson TM, Stevens B, Barres BA. Neurotoxic reactive astrocytes are induced by activated microglia. Nature. 2017. (541):481-487. doi: 10.1038/nature21029

Lourbopoulos A, Erturk A, Hellal F. Microglia in action: how aging and injury can change the brain's guardians. Frontiers in Cellular Neuroscience. 2015. (9):54. doi: 10.3389/fncel.2015.00054

Love S. Cuprizone neurotoxicity in the rat: morphologic observations. Journal of the Neurological Sciences. 1988. (84):223-237

Maciejewski-Lenoir D, Chen S, Feng L, Maki R, Bacon KB. Characterization of fractalkine in rat brain cells: Migratory and activation signals for CX3CR1-expressing microglia. J Immunol. 1999. (163):1628-1635

Monje ML, Toda H, Palmer TD. Inflammatory blockade restores adult hippocampal neurogenesis. Science. 2003. (302):1760-1765. doi: 10.1126/science.1088417

Montalban X, Hauser SL, Kappos L, Arnold DL, Bar-Or A, Comi G, de Seze J, Giovannoni G, Hartung HP, Hemmer B, Lublin F, Rammohan KW, Selmaj K, Traboulsee A, Sauter A, Masterman D, Fontoura P, Belachew S, Garren H, Mairon N, Chin P, Wolinsky JS. Ocrelizumab versus placebo in primary progressive multiple sclerosis. The New England Journal of Medicine. 2017. (376):209-220. doi: 10.1056/NEJMoa1606468

Montoya CP, Campbell-Hope LJ, Pemberton KD, Dunnet SB. The “staircase test”: a measure of independent forelimb reaching and grasping abilities in rats. J Neurosci Methods. 1991. (2-3):219-228. doi: 10.1016/0165-0270(91)90048-5

Nowacki P, Koziarska D, Masztalewicz M. Microglia and astroglia proliferation within the normal appearing white matter in histologically active and inactive multiple sclerosis. Folia Neuropathol. 2019. (57):249-257. doi:10.5114/fn.2019.88453

Ohira K, Takeuchi R, Shoji H, Miyakawa T. Fluoxetine-induced cortical adult neurogenesis. Neuropsychopharmacology. 2013. (28):909-920. doi: 10.1038/npp.2013.2

Paolicelli RC, Bolasco G, Pagani F, Maggi L, Scianni M, Panzanelli P, Giustetto M, Ferreria TA, Guiducci E, Dumas L, Ragozzino D, Gross CT. Synaptic pruning by microglia is necessary for normal brain development. Science. 2011. (333):1456-1458.

Parkhurst CN, Yang G, Ninan I, Savas JN, Yates III JR, Lafaille JJ, Hempstead BL, Littman Dr, Gan WB. Microglia promote learning-dependent synapse formation through brain-derived neurotrophic factor. Cell. 2013. (155):1596-1609. doi: 10.1016/j.cell.2013.11.030

Plemel JR, Michaels NJ, Weishaupt N, Caprariello AV, Keough MB, Rogers JA, Yukseloglu A, Lim J, Patel VV, Rawji KS, Jensen SK, Teo W, Heyne B, Whitehead SN, Stys PK, Yong VW. Mechanisms of lysophosphatidylcholine-

induced demyelination: a primary lipid disrupting myelinopathy. Glia. 2018. (66):327-347. doi: 10.1002/glia.23245

Ponomarev ED, Maresz K, Tan Y, Dittel BN. CNS-derived interleukin-4 is essential for the regulation of autoimmune inflammation and induces a state of alternative activation in microglial cells. J Neurosci. 2007. (27):10714-10721. doi: 10.1523/JNEUROSCI.1922-07.2007

Poulen G, Aloy E, Bringuier CM, Mestre-Frances N, Artus EVF, Cardoso Maida, Perez JC, Goze-Bac C, Boukhaddoui H, Lonjon N, Gerber YN, Perrin FE. Inhibiting microglia proliferation after spinal cord injury improves recovery in mice and nonhuman primates. Theranostics. 2021. (11):8640-8659. doi: 10.7150/thno.61833

Price AW, Fowler SC. Deficits in contralateral and ipsilateral forepaw motor control following unilateral motor cortical ablations in rats. Brain Research. 1981. (205):81-90.

Prinz M, Priller J. Microglia and brain macrophages in the molecular age: from origin to neuropsychiatric disease. Nature. 2014. (15):300-312. doi: 10.1038/nrn3722

Reshef R, Kreisel T, Beroukhim D, Yirmiya R. Microglia and their CX3CR1 signaling are involved in hippocampal-but not olfactory bulb-related memory and neurogenesis. Brain, Behavior, and Immunity. 2014. (41):239-250. doi:10.1016/j.bbi.2014.04.009

Ribiero-Xavier AL, Kress BT, Goldman SA, Lacerda de Menezes JR, Nedergaard M. A distinct population of microglia supports adult neurogenesis in the subventricular zone. J Neurosci. 2015. (35): 11848-11861. doi:10.1523/JNEUROSCI.1217-15.2015

Rossi JF, Yang Lu Z, Massart C, Levon K. Dynamic immune/inflammation precision medicine: The good and the bad inflammation in infection and cancer. Front Immunol. 2021. (12):595722. doi: 10.3389/fimmu.2021.595722

Schilling T, Lehmann F, Ruckert B, Eder C. Physiological mechanisms of lysophosphatidylcholine-induced de-ramification of murine microglia. J Physiol. 2004. (557):105-120.

Segal B. The diversity of encephalitogenic CD4+ T cells in multiple sclerosis and its animal models. Journal of Clinical Medicine. 2019. (8):120. doi: 10.3390/jcm8010120

Squillace M & Linden P. The lived experiences and occupational performance and satisfaction of young adults with multiple sclerosis (MS) as related to fine motor skills. The Open Journal of Occupational Therapy. 2022. (10):1-9. doi: 10.15453/2168-6408.1920

Stratoulias V, Venero JS, Tremblay ME, Joseph B. Microglial subtypes: Diversity within the microglial community. The EMBO Journal. 2019. (38):e101997. doi: 10.15252/embj.2019101997

Su F, Yi H, Xu L, Zhang Z. Fluoxetine and S-Citalopram inhibit M1 activation and promote M2 activation of microglia in vitro. Neuroscience. 2015. (294):60-68. doi: 10.1016/j.neuroscience.2015.02.028

Tan Y-L, Yuan Y, Tian L. Microglial regional heterogeneity and its role in the brain. Molecular Psychiatry. 2020. (25):351-367. doi: 10.1038/s41380-019-0609-8

Vukovic J, Colditz MJ, Blackmore DG, Ruitenberg MJ, Bartlett PF. Microglia modulate hippocampal neural precursor activity in response to exercise and aging. J Neurosci. 2012. (32):6435-6443. doi:10.1523/JNEUROSCI.5925-11.2012

Waller R, Baxter L, Fillingham DJ, Coelho S, Pozo JM, Mozumder M, Frangi AF, Ince PG, Simpson JE, Highley JR. Iba-1-/CD68+ microglia are a prominent feature of age-associated deep subcortical white matter lesions. PLoS ONE. 2019. (14):e0210888. doi: 10.1371/journal.pone.0210888

Wallin MT et al. The prevalence of MS in the United States: A population-based estimate using health claims data. Neurology. 2019. (92):e1029-e1040. doi: 10.1212/WNL.0000000000007035

Wang D, Ichiyama RM, Zhao R, Andrews MR, Fawcett JW. Chondroitinase combined with rehabilitation promotes recovery of forelimb function in rats with chronic spinal cord injury. J Neurosci. 2011. (31):9332-9344. doi:10.1523/JNEUROSCI.0983-11.201

Wang M, Xie Y, Qin D. Proteolytic cleavage of proBDNF to mBDNF in neuropsychiatric and neurodegenerative diseases. Brain Research Bulletin. 2021. (166):172-184. doi: 10.1016/j.brainresbull.2020.11.005

Wlodarczyk A, Holtman IR, Krueger M, Yogev N, Brittger J, Khorooshi R, Benmamar-Badel A, de Boer-Bergsma JJ, Martin NA, Karram K, Kramer I, Boddeke EWGM, Waisman A, Eggen BJL, Owens T. A novel microglial subset plays a key role in myelinogenesis in developing brain. EMBO Journal. 2017. (36):3292-3308. doi: 10.15252/embj.201696056

Zapolska-Downar D, Zapolski-Downar A, Modrzejewski A, Zawierta J, Naruszewicz M. Effects of ibuprofen on the synthesis of plasminogen activator inhibitor-1 in cultured endothelial cells. Med Sci Monit. 1999. (5):428-433.

Zhang J, Boska M, Zheng Y, Liu J, Fox HS, Xiong H. Minocycline attenuation of rat corpus callosum abnormality mediated by low-dose lipopolysaccharide-induced microglia activation. Journal of Neuroinflammation. 2021. (18):100. doi: 10.1186/s12974-021-02142-x